Acta Geologica Polonica, Vol. 76 (2026), No. 3, e86
DOI: 10.24425/agp.2026.158200

Anastomosing fluvial sedimentation in a foreland basin: paleoclimatic and tectonic controls on the Middle Eocene Gercus Formation, Kurdistan Region, northeastern Iraq

SABAH ABBAS MAJEED[1,2] and WALEED SHINGALY[1]

[1] *Salahaddin University-Erbil, College of Science, Department of Earth Sciences and Petroleum, Erbil-Kirkuk Road, Erbil, Kurdistan Region, Iraq;*
e-mails: sabah.majeed@su.edu.krd; waleed.aswad@su.edu.krd
[2] *University of Garmian, Civil Engineering Department, Bardasur, Kalar; Kurdistan Region, Iraq;*
e-mail: sabah.abbas@garmian.edu.krd

ABSTRACT:

Majeed, S.A. and Shingaly, W. 2026. Anastomosing fluvial sedimentation in a foreland basin: paleoclimatic and tectonic controls on the Middle Eocene Gercus Formation, Kurdistan Region, northeastern Iraq. *Acta Geologica Polonica*, **76** (3), e86

Integrated sedimentological, petrographic, mineralogical, and facies studies of the Gercus Formation reveal a tectonically influenced fluvial depositional environment responding to changing paleoclimate. Modal QFL analysis indicates a lithic-rich framework with subangular grains and low textural maturity, suggesting a proximal derivation from heterogeneous volcanic-plutonic-metamorphic-sedimentary source terrains, associated with limited transport reworking and reduced levels of chemical weathering consistent with foreland basin depositional settings. Polymictic assemblages of lithics suggest a provenance with a tectonically active and high rate of accumulation. XRD results exhibit palygorskite-dolomite patterns suggesting that the authigenic minerals present indicate a seasonal water-deficient environment with the existence of intermittent moisture. The accumulated clay mineral distributions document successive diagenetic modifications where shallow-buried sediments keep the primary illite-chlorite assemblages extracted from the physical weathering of metamorphic-igneous terranes, compared to deeply buried rock units that experienced a complete mineralogical conversion. Lateral mineralogical changes – hematite increase (northeastern Iraq – Khalakan) versus graphite accumulation (northeastern Iraq – Merade), indicate redox-limited facies successions from poorly drained floodbasin to well-drained interchannel settings. The micritic groundmass of calcareous palaeosol horizons shows local concentrations of microspar, indicating episodic water table depth (WTD) fluctuations and high evapotranspiration under a semi-arid climate with seasonally interrupted soil moisture. Six architectural elements (CH, SB, LV, CC, CS, and FF) define an anastomosing fluvial system with widespread floodplain aggradation and common crevasse channel-splay development. The existence of this architectural system, associated with calcareous pedogenic horizons, conclusively demonstrates low-gradient floodplain settings under climatic regimes varying seasonally from arid to semi-arid conditions.

Key words: Litharenite; Palygorskite; Overbank and channel facies; Anastomosing rivers; Foreland basin; Pedogenesis; Calcretes; Climatic fluctuations.

INTRODUCTION

The Gercus Formation comprises a significant stratigraphic unit exposed within the high folded zone of northeastern Iraq. It is characterized by a unique outcrop pattern that extends in a curved and discontinuous manner across the formation in the region (Text-fig. 1). Originally described by Maxon (1936) at the type section located 20 km north of Midyat in southeastern Turkey, the formation was later given a supplementary type section by Wetzel in Dohuk, northern Iraq (Bellen *et al*. 1959). The formation outcrops exclusively at the surface in the Zagros fold-thrust belt around the northeastern Arabian plate, making it an essential component for understanding the geological history of the entire tectonically active region. The formation is up to about 100–800 m thick, based on its location (Jassim and Goff 2006).

Depositional modes for the middle Eocene Gercus Formation have been widely-variably-interpreted across a series of continental and marine models, reflecting the laterally lithological variability of the formation, as well as its geographic outcrop belts through northern Iraq and the adjacent region. Continental settings have been largely documented with interpretations from arid, semi-arid oxidizing, to humid conditions (Al-Rawi 1983; Dhanonn 1988; Al-Qayim *et al*. 2008; Hussain and Aghwan 2014; Al-Juboury *et al*. 2020; Al-Juboury *et al*. 2021; Ali *et al*. 2022; Nusaif and Khwedim 2023). Turbidite deposits of marginal to deep marine origin have been recognized, on the basis of evidence from lithofacies and from carbonate-bearing intervals (Al-Mashaikie *et al*. 2013; Kadhum and Habib 2015; Al-Mashaikie and Mohammed 2017; Awad and Aslultan 2020). Transitional depositional environments have also been registered whereby freshwater fluvial assemblages were periodically interrupted by incursions of marginal to open marine water (Ameen 2006; Yeganeh *et al*. 2012; Métais *et al*. 2014; Kettanah *et al*. 2020; Hama Salih *et al*. 2022).

However, some of the suggested depositional models have been subject to much criticism; the aeolian desert pavement and dune-field interpretation (Hussain and Aghwan 2014) was challenged directly on sedimentological grounds in favor of a continental system of fluvial environments (Karim *et al*. 2018), whilst the deep marine turbidite model (Al-Mashaikie *et al.* 2013) was similarly refuted as being inconsistent with the broader stratigraphic and sedimentological framework of the formation.

The existence of these long-standing and unexplained contradictions accentuates the need for a detailed, syntectonic sedimentological reassessment of the Gercus Formation based upon comprehensive

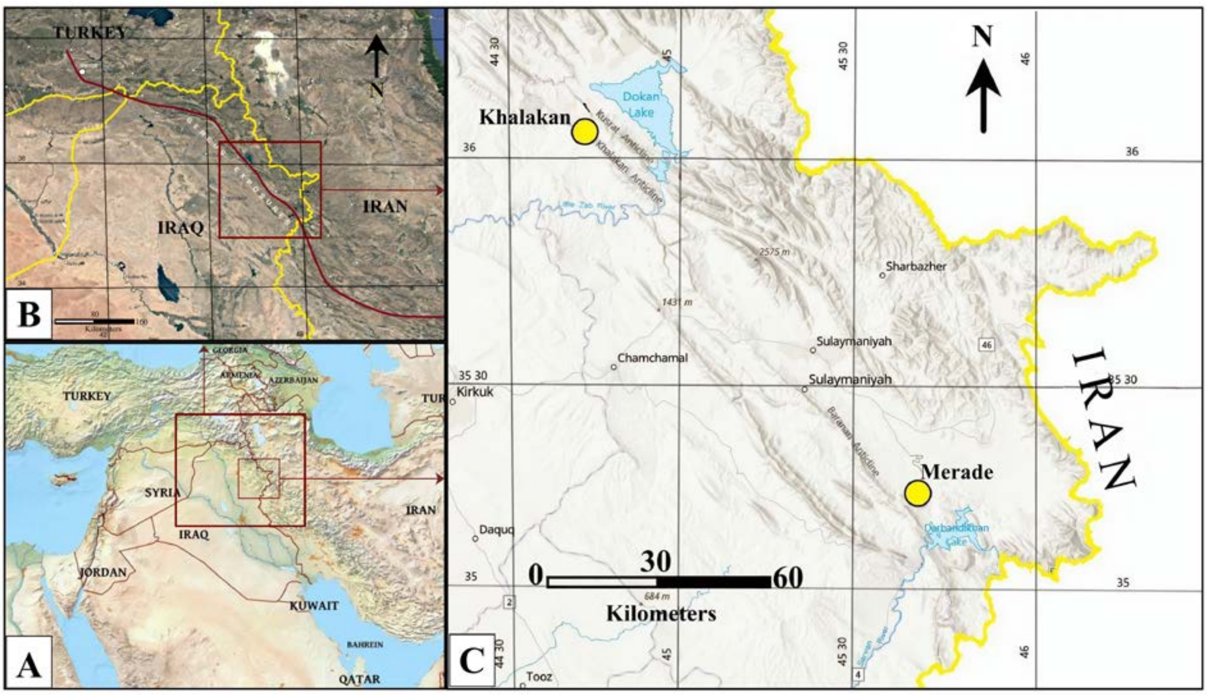

Text-fig. 1. Geographical setting of the study area: (A) Location of Iraq showing the position of the study area, Northeastern Iraq (B) Regional distribution of the Gercus Formation throughout the Zagros region (C) Detailed topographic map depicting the study positions, Northeastern Iraq (Merade and Khalakan) sections.

lithofacies characterization and configurational controls together with integrated tectonic-paleoclimatic proxies.

This ongoing disagreement concerning the depositional environment of the Gercus Formation demands further investigations with integrative sedimentological, stratigraphic and paleoenvironmental approaches. This investigation aims to offer an extensive sedimentological examination based on consistent depositional concepts and process-oriented extractions, which are expected to be related to the formation's background tectonics and paleogeography. Through a thorough reconsideration of the established views and the incorporation of new evidence, our interpretation is oriented practically to a complete understanding in regard to the deposition and environmental standpoint of this stratigraphic unit.

GEOLOGICAL SETTING

Outcropping within the High Folded Zone of the northeastern Arabian Plate, the Gercus Formation trends along arcuate structural lineaments throughout the Zagros Fold Belt (Text-fig. 2). Its basin architecture preserves the tectonic and depositional

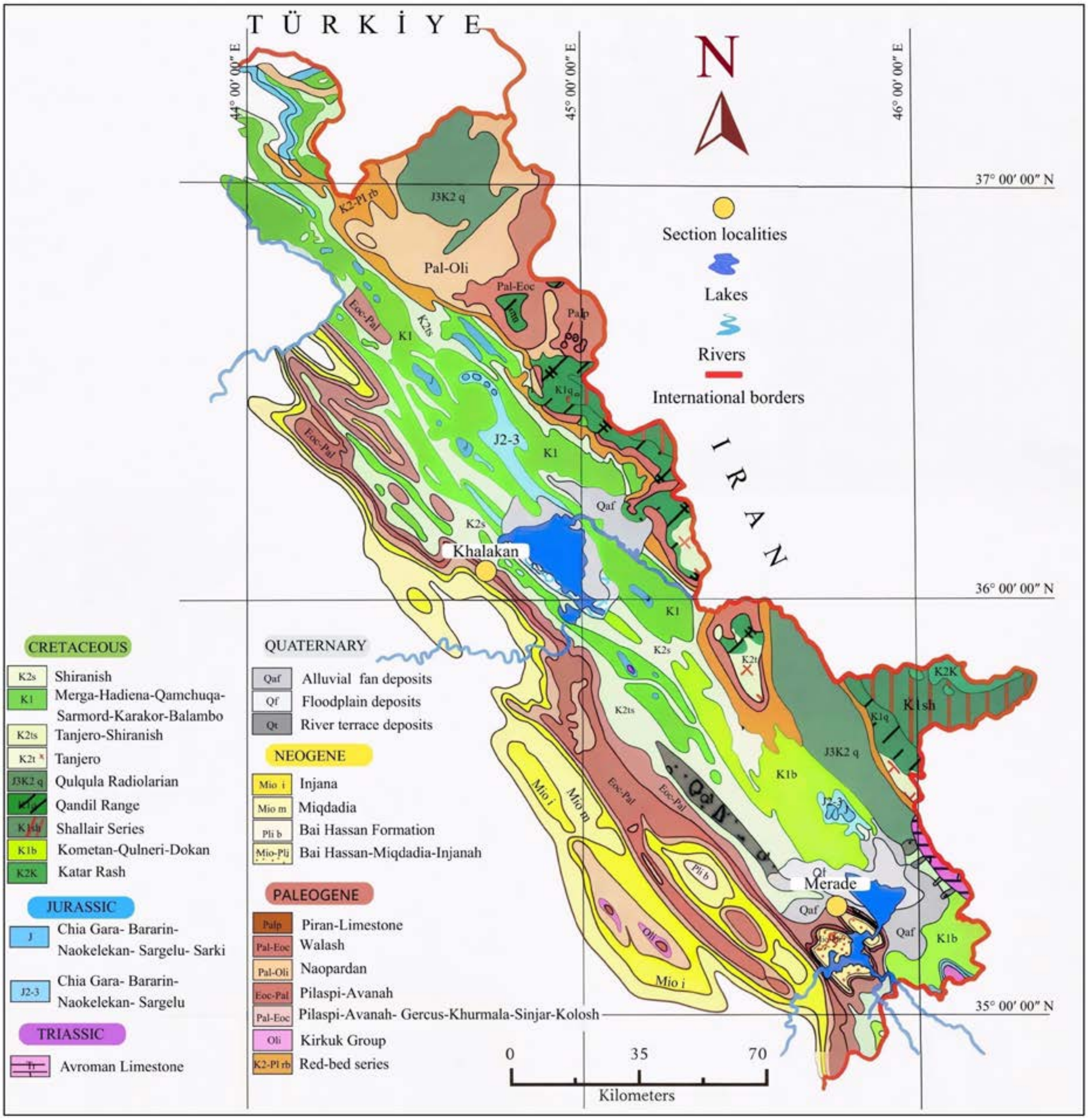

Text-fig. 2. Geological map of northeastern Iraq showing the localities of the studied sections (Modified after Iraqi Geological Survey 1986).

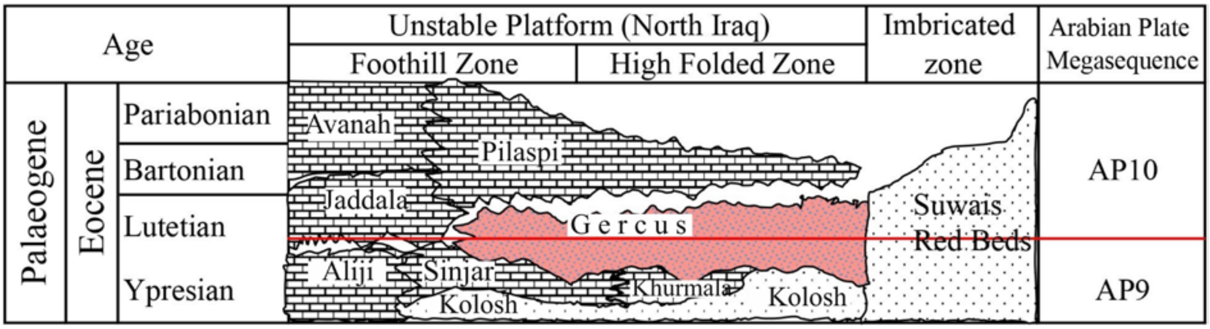

Text-fig. 3. Lithostratigraphic scheme of the Gercus Formation northern Iraq (Modified after Al-Qayim and Barzani 2021).

history of the Arabian-Eurasian plate convergence during Palaeocene–Eocene times that was associated with the construction of a magmatic arc due to closure of the Neo-Tethys Ocean as part of the AP10 Megasequence, leading to systematic uplift across the northeastern Arabian Plate. This structuring resulted in a ridge-and basin structure, which had an effect on the fluvial-marine systems of deposition (Jassim and Goff 2006). The basin was a dynamic sedimentary system driven by active tectonism and simultaneous Middle Eocene sedimentation, and] in the upper Peshdar Stock (Scotese 2014), widespread clastic deposition is seen, reflecting the vertical subsidence of the Zagros orogenic wedge. The studied stratigraphic sections are situated in the northeastern part of the Zagros High Folded Zone (Text-fig. 3). Present here are the following two representative and continuously exposed outcrop localities, the Merade section, near Darbandikhan, and the Khalakan section, at the Dokan location.

– The Merade Section: This section is located in Merade village, which is situated about 20 km north of the Darbandikhan district, southern Sulaymaniyah Governorate. The section can be viewed from the Darbandikhan reservoir at 35°14’36.0“N, 45°41’19.0“E, 700 m a.s.l. Stratigraphic exposure occurs on the limb of an overturned anticline, which is located about 1400 m north of the Baranan anticline. It is positioned in a structurally complex domain at the onset of the High Folded Zone (Text-fig. 1).
– The Khalakan Section: This section is located in Rubar village, proximal to the Khalakan subdistrict, and is situated on the Khalakan Anticline (36°03’06”N, 44°46’21”E; 1000 m a.s.l.). The section is exposed on the eastern limb of the Khalakan Anticline, opposite the Kusrat Anticline. The Gercus Formation outcrops on the upper and lateral portions of the anticline and reaches approximately 62 m in thickness (Text-fig. 1).

Stratigraphically, the study area is located within the Palaeocene–Eocene AP10 Megasequence of the Zagros High Folded Belt (Sharland *et al.* 2001), and it is situated between the underlying Sinjar Formation and the overlying Pilaspi Formation which form its base and top horizons respectively, (Text-fig. 2) is a comprehensive map of the geological successions of the studied area, ranging from Quaternary to Triassic periods, and (Text fig. 3) illustrates the stratigraphic position of the Gercus Formation. The base of this formation shows a gradational relationship with the Sinjar Formation in recrystallized limestone facies (Keller 1941; Bellen *et al.* 1959), whereas across the highly folded belt between the Gercus and Fatha Formations, the Pilaspi Formation is stratigraphically sandwiched between them (Al-Qayim *et al.* 2012; Sissakian and Fouad 2015), showing an unconformable upper contact on the Gercus Formation.

MATERIALS AND METHODS

This study employed and conducted integrated sedimentological fieldwork and laboratory analysis, characterizing lithological, granulometric, petrographic, and facies analyses of the Gercus formation.

Lithological discontinuities defined stratigraphic boundaries. Bed thickness measurements followed the methodology of Jacob’s staff, with corrections applied for structural dip to ensure stratigraphic accuracy. Lithological descriptions and field sampling for each bed were made, involving color, grading, sedimentary structures, sorting degree, surficial features, and grain size through the naked eye and hand lens. Representative samples were collected systematically for genetic types and sediment source analysis. Grain size analysis samples were manually disaggregated to reduce over-pulverization. Coarse fractions were separated through dry sieving, while

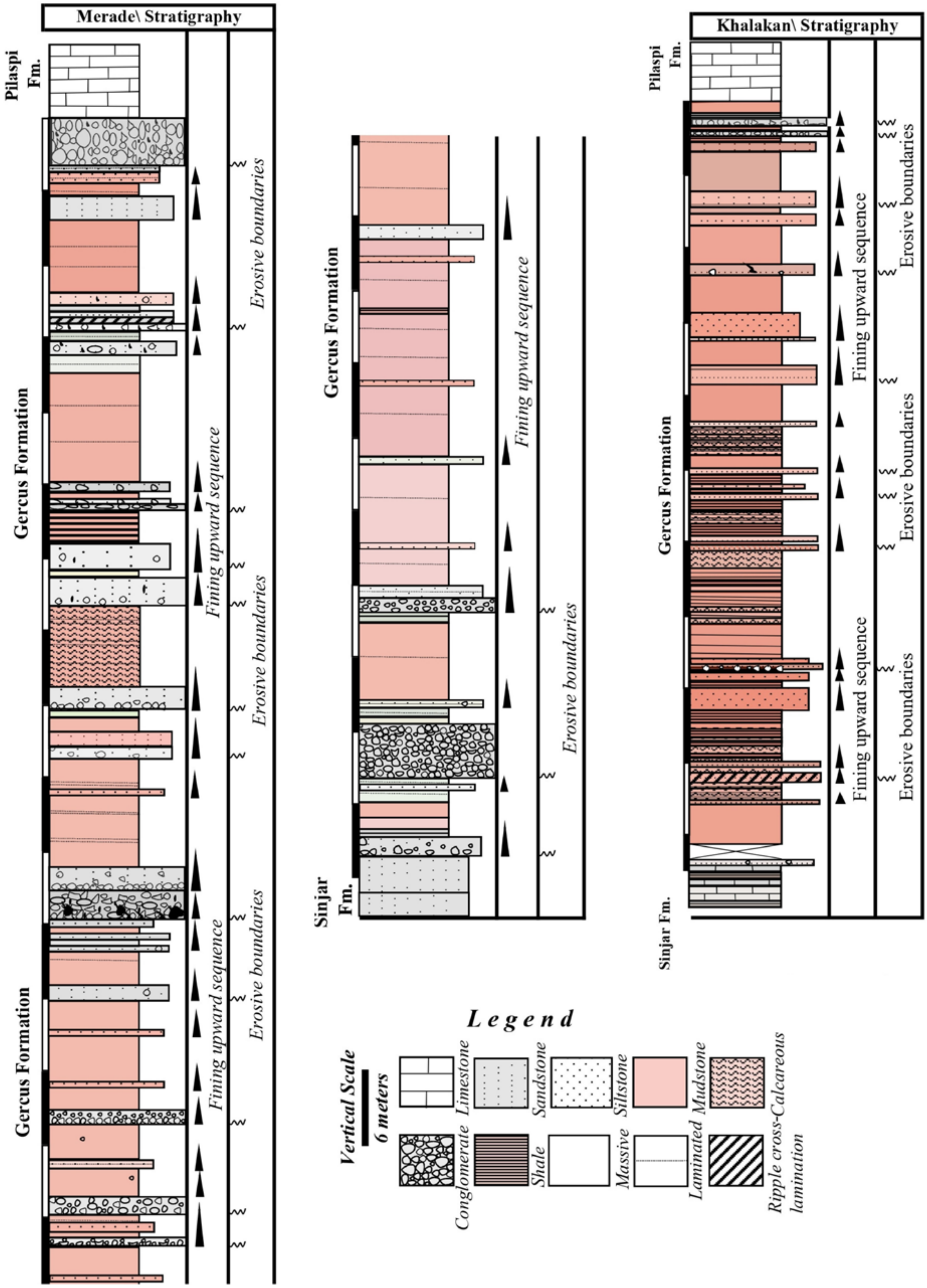

Text-fig. 4. Stratigraphy logs of the study sections representing lithology, finning-upward trends, and erosive bed contacts.

fine-grained specimens were soaked to induce disaggregation of the less than 62 μm fine-grained matrix. The fine fractions were analyzed using hydrometer methods. These grain-aggregation separation methods were basically used to characterize the sedimentary texture and to later support the facies interpretation. In petrographic analysis of 15 lithic wacke and lithic arenite thin sections, 400 points were counted by PLM per slide, then averaged to give the percentage. Framework grain compositions were quantified in randomized patterns using JMicro-Vision and Image-J software. The X-Ray diffraction (XRD) method was done for eight rock samples in the selected sections.

Four-mud and fine-grained samples were chosen for mineralogical analysis representing lithological variations within selected intervals. An additional four samples were used for analyzing clay mineral assemblages within the mudstone and shale horizons.

The clay-mineral samples underwent three standard steps. In step 1, drilled oriented clay specimens were analyzed in an air-dried condition to obtain baseline d-spacing values. In step 2, the same samples were exposed to ethylene glycol vapor for 12–24 hours and re-scanned to reveal expandable clay minerals. In step 3, the specimens were baked at 550°C for two hours and re-analyzed to separate kaolinite from other clay types via collapse patterns.

LITHOSTRATIGRAPHIC FRAMEWORK AND FIELD OBSERVATIONS

Lithostratigraphic analysis provides a fundamental framework in sedimentary basin studies, and it serves as the cornerstone for reconstructing basin evolution and paleoenvironmental reconstruction (Salvador 2013; Catuneanu 2019). Such studies generally combine field observations, petrographic data, and sedimentological interpretation to enable characterization of vertical and lateral lithologic relations. By these means, the lithostratigraphy facilitates the interpretation of depositional systems (facies transitions), provenance variations, and tectonostratigraphic history across disparate basin settings (Miall 2016; Nichols 2023).

To characterize the textural variations and sedimentary structures, bed-by-bed systematic documentation was conducted at two outcrop localities. The Merade and Khalakan sections reside stratigraphically between the Sinjar and Pilaspi formations (Text-fig. 3) and are entirely siliciclastic successions encompassing lithologies that are reddish-brown, grey, and green claystone, shale, mudstone, siltstone, sandstone, and conglomerate. The Khalakan section has more prominent fine-grained lithologies, including a substantial amount of interbedded mudstone, while coarse-grained facies are subordinate. The conglomeratic intervals occasionally show fining-upward sequences with a heterogeneous grain-size distribution from sand to cobbles. The measured thickness at each section was 160 m and 62 m for Merade and Khalakan, respectively (Text-fig. 4).

Field observations reveal a gradational, interbedded lower contact of the Gercus with the underlying Sinjar Formation, including a 2-m-thick conglomeratic sandstone. The upper contact is an unconformable clast-supported conglomerate, as recognized in the Merade section. Fine-grained lithologies are common occurrences, and they account for 78% of the succession in Merade and an even higher percentage in Khalakan. Such horizons typically show a thickness from a centimeter to 4 m. Sediments from fine-grained lithologies have well-developed, weak stratification and parallel laminations and are occasionally interbedded with siltstone. Their primary sedimentary features are usually destroyed through compaction and deformation. The fine-grained facies tends to display a stronger lateral continuity.

Blocky-conchoidal shapes form subangular to irregular ped structures, identified in fine-grained intervals, particularly in the white-to-grey-to-reddish-brown horizons (Text-fig. 5A). Pale mottling features, root traces and nodules of pedogenic carbonate accumulations are found in both sections (Text-fig. 5G, H). Mudstone horizons are typically limited to the Khalakan section and are rhythmically interbedded, indurated, and display isolated parallel-laminated horizons among fissile shales (Text-fig. 5B). In the Merade section, dispersed extraformational clasts within fine-grained strata at 10–100 cm intervals indicate high-magnitude flood event variations (Text-fig. 5C).

Text-fig. 5. Field photographs (A) Blocky-subangular and conchoidal structures of pedogenic muddy horizon, SC: KhG28, Khalakan, (B) Alternation parasequences of mudstone, siltstone, and shale; yellow tape is 60 cm, SC: KhG22, Khalakan, (C) Oriented isolated gravel clasts within pedogenic mudstone, SC: MG27, Merade, (D) Rip-up clast preservation of fine-grained (yellow arrows) within bituminous conglomeratic horizon, SC: MG34, Merade, (E) Erosive boundary and scour fill structure at the conglomeratic basal lag, SC: MG26, Merade, (F) Fining-upward sequence of a conglomerate (lower) and conglomeratic sandstone (upper) horizon, gradually fining-up into sandstone and mudstone horizons, SC: MG43, Merade. Note: SC= sample code. The hammer scale is 30 cm. (G) mottling (white spots) and rootlet features (yellow arrows), within the pinkish-red mudstone, SC: MG42, Merade, (H) Redoximorphic mottling, blotchy color within the mudstone, SC: MG20, Merade. →

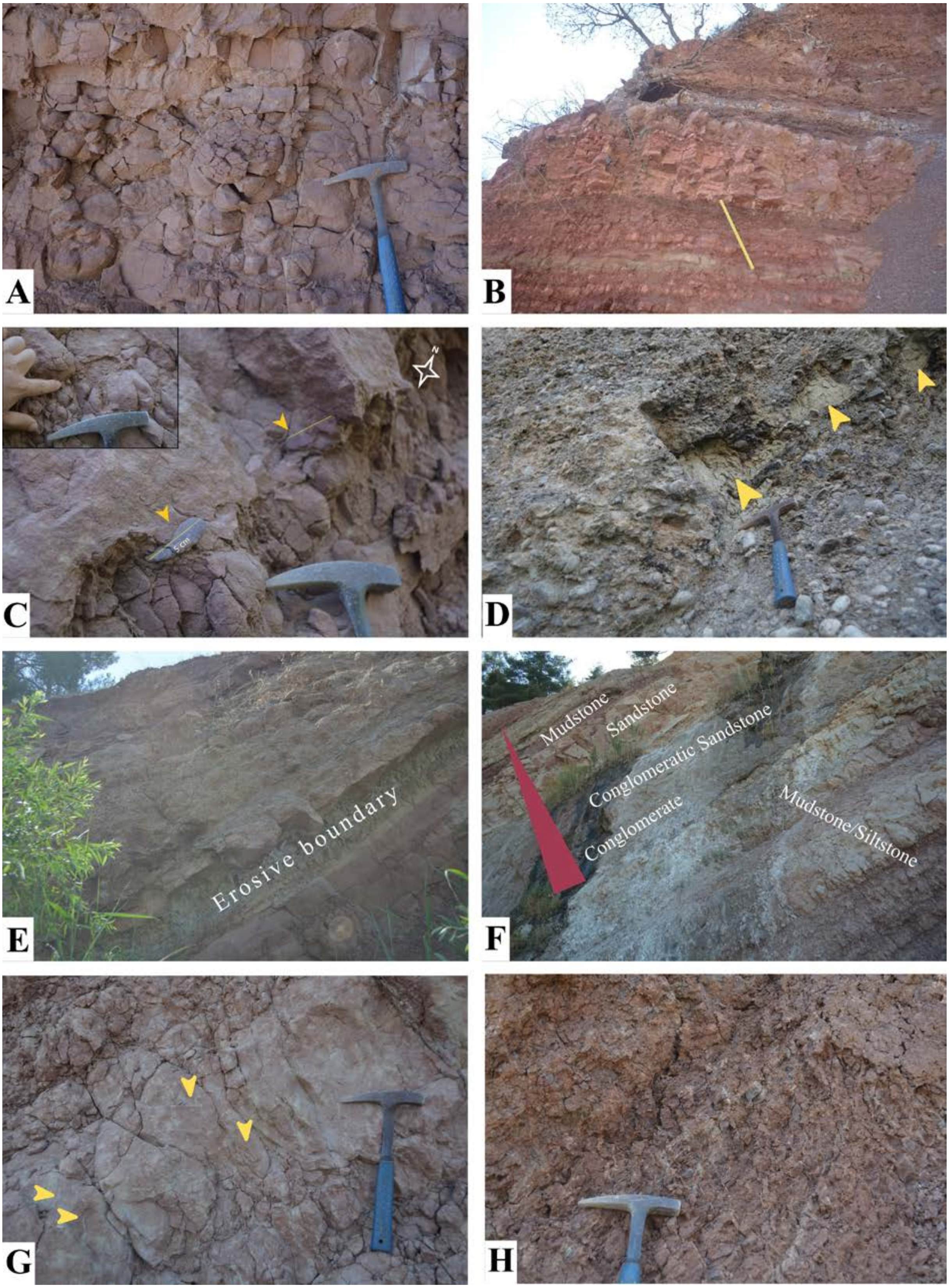
A
B
C
D
E
Erosive boundary
F
Mudstone
Sandstone
Conglomeratic Sandstone
Conglomerate
Mudstone/Siltstone
G
H

Sandstone horizons show reddish-brown, grey, greenish, and yellowish coloration and are medium to fine-grained, made up of well- to moderately sorted grains. Sedimentary structures within sandstone horizons include massive bedding, planar lamination, ripple lamination, and low-angle cross-stratification, characterized by distinguished flames of erosion. Sandstone bed thickness ranges from 20 cm to 2 m. Conglomeratic lithofacies total 12% in the Merade and 2% in the Khalakan section and are made up of heterogeneous granulometric (granule-boulder) clasts with a sandy-silty matrix, characterized by angular-to-rounded morphologies, very poor sorting, normal grading, massive and scour-fill geometries, with basal surfaces presenting rip-up clasts, lag deposits, and bitumen impregnation (Text-fig. 5D). The thickness of conglomeratic horizons varies from 25 cm to 4.5 m; sharp, concave-upward erosional surfaces cut conglomerate bases in the Merade section. They truncate underlying fine-grained units while being bounded by erosional surfaces and being capped by extensive mudstone intervals of fining-upward sequences (Text-fig. 5E, D).

At the base of the conglomeratic horizons, particularly in the Merade section, multiple erosive bed boundaries are observed. They are sharp, concave-up basal geometries, synchronized with rip-up clasts and underlying mud, silt, and shale units (Text-figs 4 and 5D). Fining-upward sequences are a distinct feature of the succession and they are linked with the basal erosional boundaries, as shown in (Text-fig. 4). This sequence represents a systematic reduction in grain size, starting with basal lag and gradually decreasing into sand, silt, and mud horizons. These sequences are typically situated between extensive mudstone strata (Text-fig. 5E, F).

FACIES ANALYSIS AND DEPOSITIONAL ARCHITECTURE

Facies classification

Facies analysis is an essential foundational basis in sedimentology that plays a significant role in reconstructing the depositional processes, paleoenvironmental conditions, and basin-fill architecture based on systematic observation of lithological characteristics and sedimentary structures (Reading 1996; Miall 2016). Lithofacies are spatially discrete (in terms of the arrangement over the area surveyed) mappable sedimentary units with unique pertinent textural and compositional properties that can serve as a proxy indicative of specific depositional mechanisms and hydraulic regimes (Walker and James 1992; Miall 2006). Modern facies model formation has focused on combining the lithofacies properties with their three-dimensional geometrical relationships and stacking patterns in a geologically realistic manner to improve predictive ability related to basin development and sediment transfer dynamics (Posamentier and Walker 2006; Miall 2016).

The distinctive lithofacies of the Gercus Formation is clearly distinguishable from the underlying Sinjar Formation and the overlying Pliaspi Formation due the presence of depositional breaks representative by conglomerate at the upper contact, while there is a clear gradational facies at the Sinjar lower contact. In the studied sections, the Formation has been lithofacially assembled into twelve distinct facies types on the basis of diagnostic sedimentological criteria, including grain-size distribution, mineralogical composition, texture maturity, grade bedding architecture, and physical sedimentary structures (Table 1; Text-fig. 6).

Facies A: Matrix-Supported Conglomerate: This facies is a matrix-supported conglomerate, with low grading (sometimes no grading), and without clast imbrication, the isolated clasts being dispersed in a fine-grained matrix that exceeds 15% of the volume. The thickness of individual horizons varies from 0.2 to 4.5 m (Text-fig. 7A). This facies is equivalent to Miall's (2016) lithofacies code Gmm, which was interpreted as a product of debris flow or sheet flow in high-strength flows.

Facies B: Massive to Crudely Stratified Graded Conglomerate: This is composed of a matrix-supported conglomerate, with the clasts dispersed in a sandy-muddy matrix. Bedding is massive to crudely stratified at the base: vertical sections show normal and rare inverse grading near the basal contact. Individual horizons are 0.2 to 2.5 m thick and have lenticular geometries, with erosive basal surfaces cutting down into underlying strata (Text-fig. 7B). This facies is comparable to Miall's (2016) lithofacies code Gmg.

Facies C: Clast-Supported Massive Conglomerate: This facies consists of clast-supported conglomerate containing pebble- to cobble-sized clasts and occasional boulder-sized constituents. The interstitial matrix material, comprising particles of sand size and mud, is less than 15% by volume. The horizon is lenticular in geometry and between a few decimeters and 2 m thick with low lateral continuity (Text-

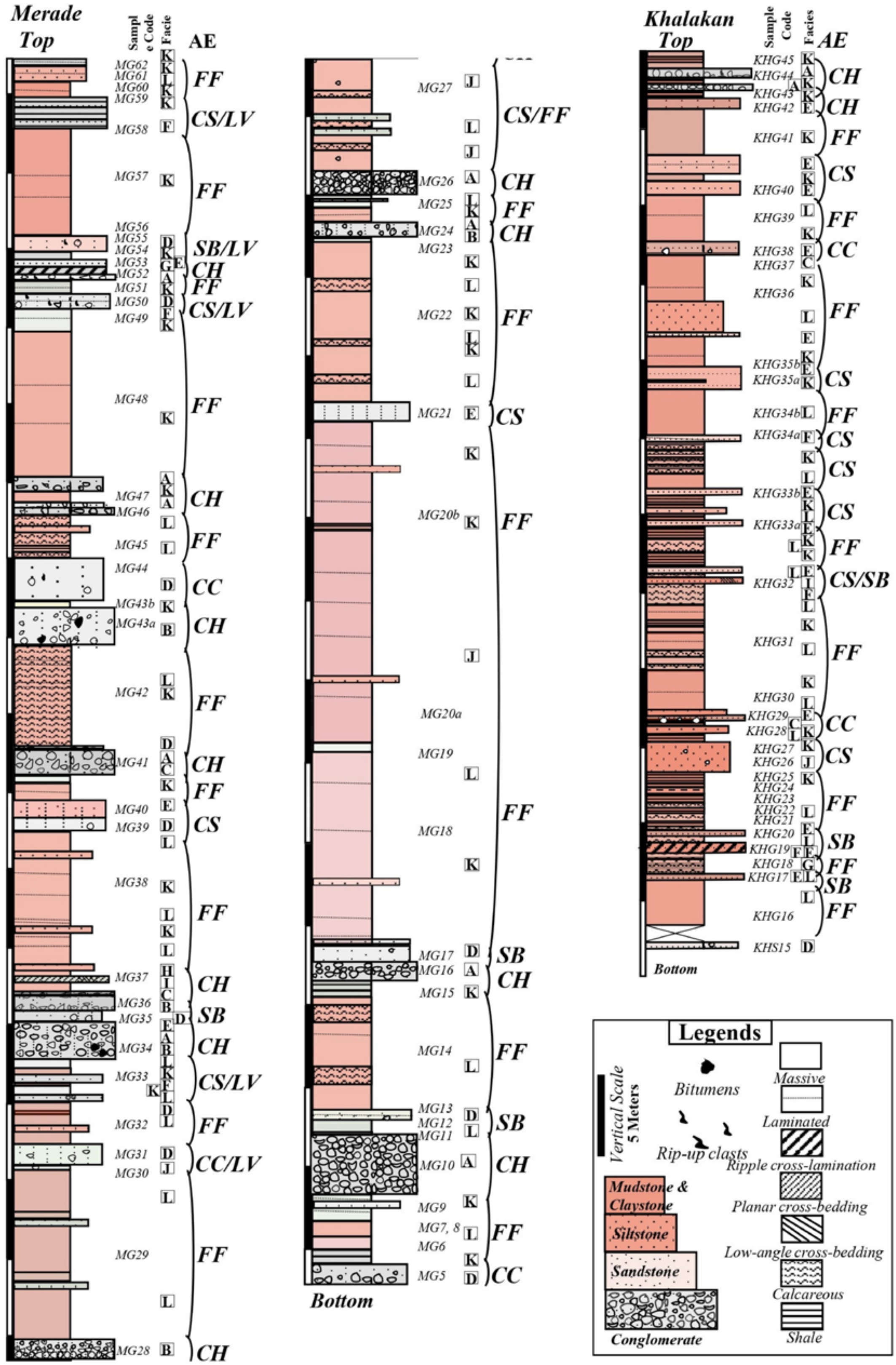

Text-fig. 6. Stratigraphic logs of the sections, showing Lithofacies (on the left), and architecture elements (on the right); look at the Tables 1 and 2 for the symbols.

Facies	Lithofacies	Description	Sedimentary structures	Facies codes	Interpretation
A	matrix-supported conglomerate, matrix >15%	dark-grey, v. poor to poorly sorted, pebble to cobble clasts, subangular to subrounded shapes, sharp base	massive, weak grading, rip-up clast	Gmm	debris flow, channel fills, flood-flow deposits, scour fills
B	matrix-supported conglomerate, matrix >15%	grey, v. poorly sorted, rounded to sub-rounded clasts, sharp basal surfaces, leaks of bitumen	inverse to normal grading	Gmg	debris flow, debris-laden floods
C	clast-supported conglomerate, matrix <15%	grey, large clasts, sub-rounded to rounded, poor-to-moderate sorting	massive pebble	Gcm	debris flow (inertial bedload, turbulent flow), scour fills
D	coarse to fine sandstone with gravel	greenish-grey, dark-grey, coarse- to fine-grained, moderately-to-poorly sorted, sharp basal contact	massive, lenticular bedding, small scour fill, weak normal-reverse grading	Sg	turbated sand, bar-front flows, traction and short suspension, flood sheets, proximal channel fills
E	fine to coarse sandstone	light-dark-grey to reddish-brown, coarse- to fine sand, moderately to well sorted, erosive contact	massive, faint lamination, scours	Sm	gravity flow deposits, scour fills
F	fine to coarse sandstone, pebbly	grey-brown, moderate- to well-sorted, sharp-gradational basal contact	lamination, streaming lineation	Sh	Plane-bed flow (critical flow)
G	fine to coarse sandstone	enduring, grey-to-reddish brown moderate-to-good sorting, subrounded to rounded, erosive basal	climbing ripples, ripple cross-laminated	Sr	lower-flow-regime ripple migration, high fallout rate of suspended and traction sand
H	fine to coarse sandstone	pale-yellow, moderately sorted, basal and the upper contacts are sharp	planar cross-bedding	Sp	migration of 2-D dunes under unidirectional current flow
I	fine to medium sandstone	reddish-brown, moderately sorting, indurated, angular-to sub-rounded, gradual basal contact, sharp to the upper contact	low-angle cross-bedded	Sl	sandy bedforms within a channel (CH) belt
J	mudstone to medium and fine sandstone, pebbly	reddish-brown, fine-sand, mud, scattered gravels, moderately sorted, rugged and blocky fabric, polygonal shapes of cracking	massive	Fm (g)	suspension fall-out of fines from waning overbank flows, debris-flood / hyperconcentrated splay
K	mudstone, silt, clay	pale brown- gray-to-reddish brown, stark parallel and laminated beds, fissile, thin laminae	lamination	Fl	quiet-water, suspension fallout on floodplains, settling from waning overbank flows
L	mudstone, silt, clay	reddish-brown to litght-grey-white clay-silt grade, blocky, pedogenic, calcrete nodules, irregular contacts	massive, structureless, desiccation cracks, calcareous, pedogenic calcrete	Fm, Fm (p-cal)	suspension of mud on a low-energy floodplain, episodic flooding and subaerial exposure

Table 1. Facies classification of Gercus formation in the study sections.

fig. 7C). This facies is uncommon in the stratigraphic successions. It relates to Miall's (2016) lithofacies code Gcm, described as very high-energy flow deposits near sediment sources.

Facies D: Gravelly Massive Sandstone: This facies is composed of large and thick bedded units. There are localized normal gradings and minor, subordinate reverse gradings. Bed geometry ranges from tabular to lenticular with sharp, erosive basal contacts indicative of sheet-flow burial. The clasts are subrounded to rounded in shape, randomly oriented. The horizon thickness ranges from 0.2 to 2.5 m, this facies is more common at the Merade section (Text-fig. 7D).

Facies E: Massive Sandstone; locally with reddish-brown mottling, which is often of very coarse

Text-fig. 7. Facies photographs. (A) Matrix-supported conglomerate, massive, facies A, MG16; (B) Matrix-supported conglomerate, normal grading, facies B, MG28; (C) Clast-supported conglomerate, massive, facies C, MG41; (D) Gravelly sandstone, massive and laminated, facies D, MG44; (E) Massive sandstone, facies E, KhG41; (F) Laminated sandstone, facies F, MG58; (G) Ripple cross-laminated sandstone, facies G, KhG19; (H) Planar cross-bedding sandstone, facies H, MG38; (I) Low-angle cross-bedded sandstone, facies I, KhG32; (J) Gravelly massive mudstone, facies J, MG27; (K) Laminated mudstone, facies K, MG51; (L) Massive, calcareous, pedogenic mudstone, facies L, KhG32, (M) Hypocoating pedogenic carbonate (Calcisol), KhG32, (N) Root tubules, fossilized root replaced by calcite, and mottling signatures, KhG33. Notes: 1. Codes are related to the sample codes, 2. Hammer scale is 30 cm, 3. Length of the yellow tape is 60 cm. →

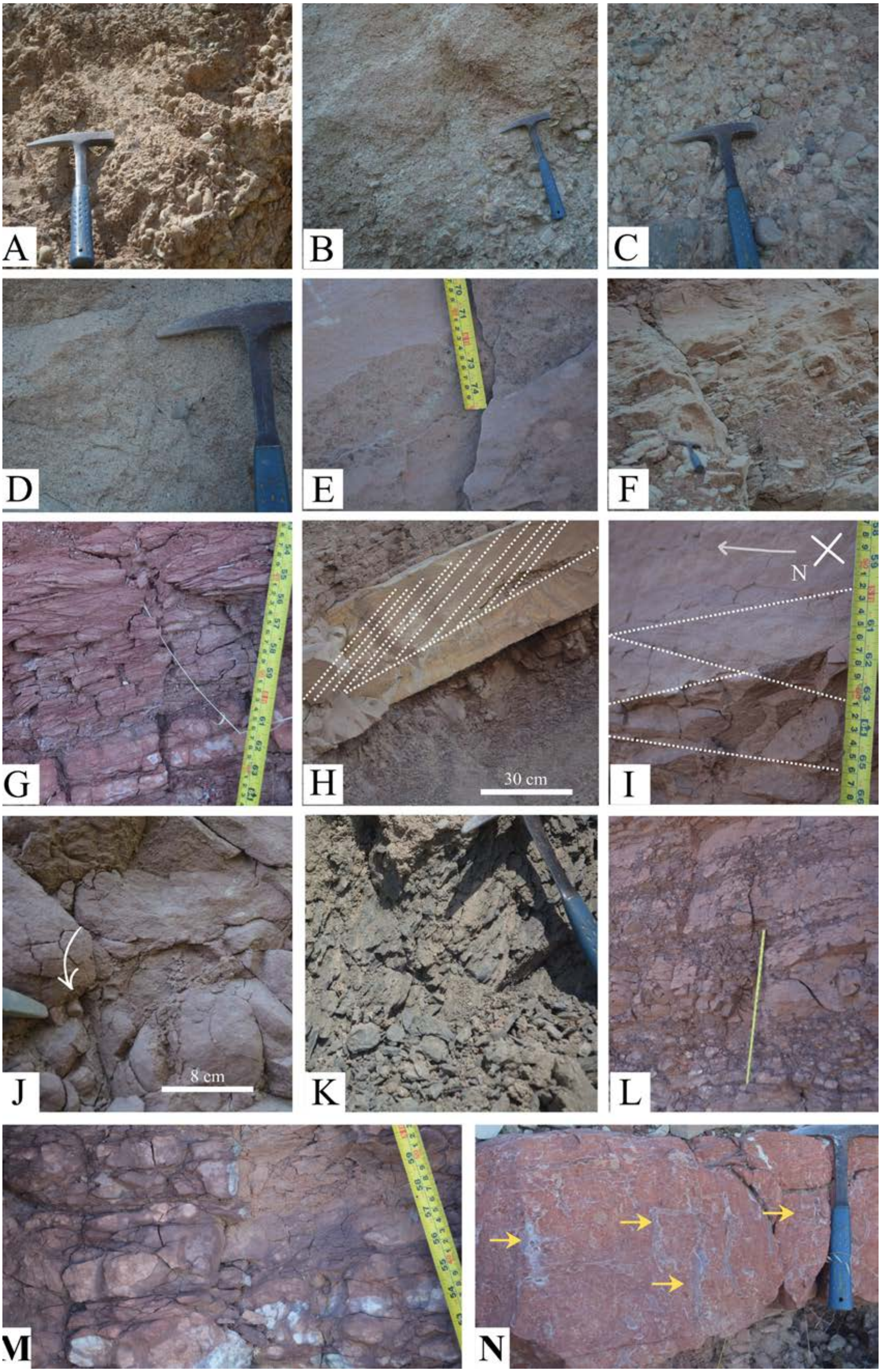
A
B
C
D
E
F
G
H
30 cm
I
N
J
8 cm
K
L
M
N

grain size at the bed bases, with a matrix-supported texture. Mud rip-up clasts are rare, and ephemeral lamination is locally present. The beds are tabular to lenticular in geometry, with sharp to slightly erosive basal contacts, and they can range in thickness from a few cm to 1.5 m. This facies is abundant in both sections and is equivalent to Miall's (2016) lithofacies code Sm (Text-fig. 7E).

Facies F: Horizontally Laminated Sandstone: this facies has planar parallel laminae bedding planes which have lateral continuity with low-angle scour surfaces. There are sparse granule or isolated clast stringers, which are discontinuous and restricted to discrete laminae, occurring as a pebbly variant, Sh(g), but over only 20 cm thickness (Text-fig. 7F). The lithofacies code for this facies is Sh (Miall 1996, 2016).

Facies G: Ripple Cross-Laminated Sandstone: This is arranged in mm-thick foreset laminae. The inner laminae are tangential at the base and downlap onto underlying stoss surfaces, locally developing climbing-ripple fabrics. The laminations show pinch-and-swell geometries and subtle aggradation. Beds are tabular to gently lenticular. This facies is illustrated from both sections with climbing-ripples in the Khalakan and Merade sections and three-dimensional festoon ripple sets at Khalakan (Text-fig. 7G). It can be corresponded to Miall's (1996, 2016) lithofacies code Sr.

Facies H: Planer Cross-Bedded Sandstone: This is represented by a single, lens-shaped bed that is 45 cm thick and tabular to slightly wedge-shaped, with the lower contact clearly of erosive nature. The facies shows coarsening upward to coarse grains in wrinkled and rucked-base lag. Foresets are formed by subparallel laminae dipping at about 20° with paleocurrent direction from south to north (Text-fig. 7H). According to Miall (1996), this facies is correlated with lithofacies code Sp and interpreted as a channel belt fill associated with the migration of sandy bars.

Facies I: Low-Angle Cross-Bedded Sandstone: This facies is locally found in Sh sheets sandstone (in the Khalakan section). It is formed of one tabular bed (c. 20 cm), (Text-fig. 7I). Flow direction to the northwest is indicated by paleocurrent data. In accordance with Miall (1985, 1996) and Bridge (2003), the facies was interpreted to have been deposited on the lee side of sandy bars in a fluvial-channel belt.

Facies J: Pebbly Massive Mudstone: This facies contains scattered granule- to pebble-sized (1–3 cm) clasts without preferential orientation, with polygonal cracking (caused by desiccation) superimposed upon palaeosol modification, mottling signatures and calcrete (Text-fig. 7J). This facies is rarer and very well recorded in the two sections as thick beds intercalated with conglomeratic units. It is correlated with lithofacies code Fm(g).

Facies K: Horizontally Laminated Mudstone: This facies consists of shale, mudstone, fine sandstone and lamination together with wispy silty to sandy streaks. Horizons are tabular in form, cm to decimeters thick with sharp contacts, and laterally can be traced over meters. Mottle patterns, root traces, and calcretes are usually recorded in this facies. The mottles are interpreted as characterizing redoximorphic status which alternates between oxidizing and reducing microenvironment conditions and can be an indicator of waterlogged floodplain paleosols (Kraus 1999; Retallack 2001). Mottles occur as blotchy color heterogeneity within the mudstone horizon. Rootlets show irregular vertical to subvertical stripes with visible tubular voids. Calcrete carbonate nodules recognized by their reddish brown-pale creamy-grey dark-colors, and irregular texture point to calcisol developed in seasonally flooded zones (Text-figs 5H and 7K, M). A calcisol is a pedogenic mature palaeosol, which shows pronounced secondary accumulation of calcium carbonate within the soil profile (Akça *et al.* 2018). This facies is common throughout the sections and frequently occurs for tens of meters vertically. It is equivalent to Miall's (2016) lithofacies code Fl.

Facies L: Massive Mudstone: Structureless horizons are mainly characterized by coarsely massive, blocky, and rubbly pedogenic aggregates. White nodules\hypocoatings calcretes visible in the mudstone are interpreted as large calcisol developed under contrasting wet\dry climate on the stable floodplain surfaces (Text-fig. 7L, M). Fossiliferous root traces found in this facies, replaced by calcite in the oxidized muddy matrix are interpreted as pedogenic carbonate. (Text-figs 7N and 5G). Several horizons show calcretes, rootlets, mottling, and desiccation cracks. Bed thickness varies from decimeters to meters. This facies commonly re-occurs throughout the stratigraphic sequence. According to Miall's (1996, 2016) classification, it is code type Fm, and the lithofacies arrow is Fm (p-calc) for palaeosol calcrete nodules (Text-fig. 7L). Facies L is also well-documented in the Khalakan section.

Architecture elements (AE)

This application subdivides sedimentary successions into a hierarchy of 3-D rock units; each unit is bounded by erosional or accretionary surfaces of different orders. This hierarchical analysis improves and sharpens the description of the lithofacies altogether within the elements. Each element clarifies the time duration and spatial extent of the controlling depositional processes (Miall 1985, 1996, 2014). Facies classification in the present study is based on assemblage relationships deduced from macroform morphology and stratigraphic architecture. Six architectural elements are identified in the Gercus Formation on the basis of bounding surface type, geometry of bedding, paleocurrent/stratigraphic indicators, and stacking patterns (Table 2; Text-figs 6 and 8).

Channel Fills Element (CH): Comprises facies (A, B, C) with subordinate sets of facies (D, E, H, I) covered and underlain by (K and L) facies. Channel fills are characterized by concave-up geometry, erosional bases, occasional bounding by floodplain sediments, and vertical stacking, showing low-angle accretion. This element frequently occurs throughout the Merade section, from the base to the top (Text-fig. 8A).

Sandy Bedforms (SB): Ephemeral sediments primarily composed of sandy facies with scattered gravels (E, D), occasionally with subordinate facies (F, G, H, I). This element is typically overlain by thinly bedded, sheet-like finer sediments of the floodplain or showing fining upward deposits and occasionally situated between main channel fills. Sandy bedform elements display massive, rippled laminated structures, low-angle cross-bedded sandstone, wedges or have lenticular geometries and vertical stacking. Sandy Bedforms elements sometime have an erosive boundary at the base and occasionally co-occur with crevasse splay deposits (CS). This element is found in both sections (Text-fig. 8A, B).

Levee Elements (LV): Comprise facies (F, G, K, L) and represent rhythmic units of muddy to fine laminated sandstone. Each rhythmic bed within the levee element shows a flood event (Miall 2016). This element is frequently observed in the Merade section,

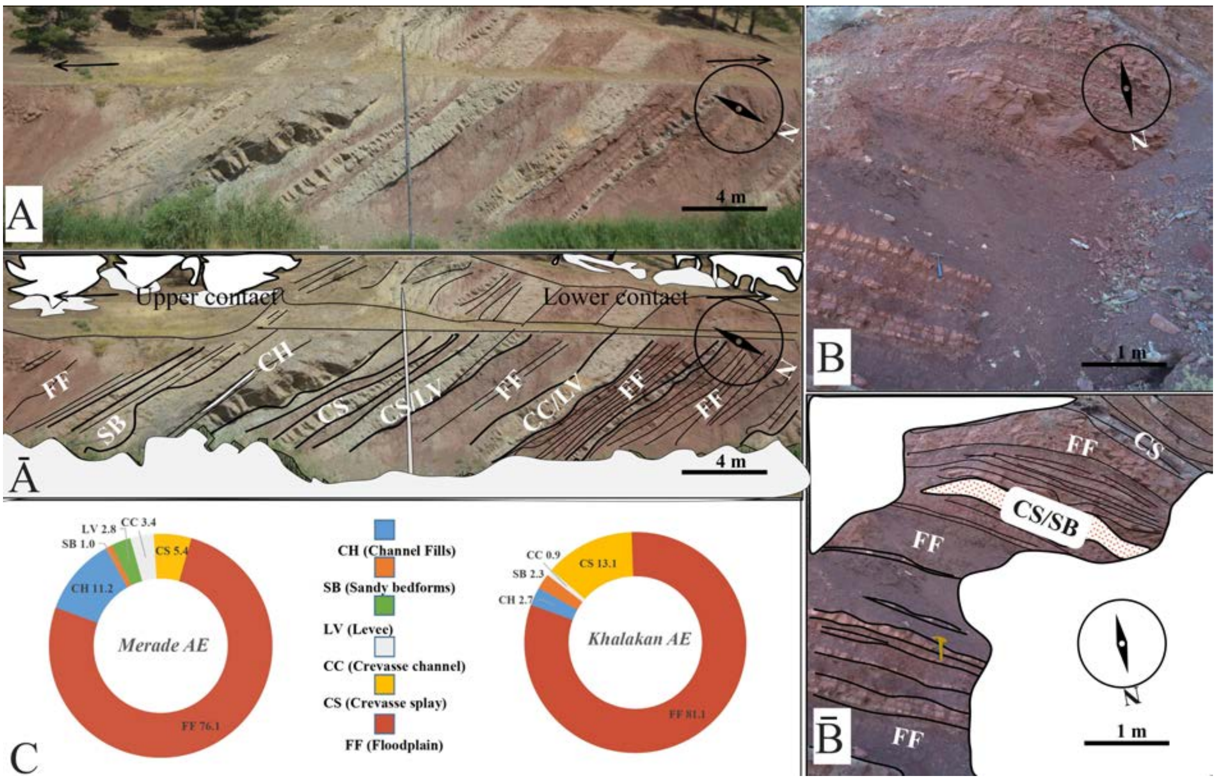

Text-fig. 8. Architecture elements (AE) of the Gercus Formation (A, Ā) panoramic and schematic photographs show vertical and lateral relationships of the Merade architectural elements, (B, B̄) vertical architecture elements relationships of the Khalakan section. (C) Frequency of various architectural elements (AE) occurrence in the studied sections. Channel-fill elements (CH, and SB) occupy a minor ratio of the total thickness. Overbank elements (LV, CC, CS, and FF) make up major ratio about 91% (average) of the total thickness.

Element		Symbol	Facies assemblages	Interpretation
Channel-fill element	Channel fills	CH	C, A, B, minor D, E, H, I, K, L	Main channel fills and reoccupation, high-energy thalweg deposits (Bridge 2003; Miall 2016).
	Sandy bedforms	SB	E, D, Minor F, G, H	Bed-form bursts in channels; typically thin lenses interfingered with mud-rich beds (Allen 1982; Southard 1991).
Overbank element	Levee	LV	F, E, G, K, L	Repeated overbank pulse-formed builds; laterally continuous mud with subtle sand pinstripes, forming during flood stages (Reineck and Singh 1980; Bridge 2003).
	Crevasse channel	CC	E, D, C, F, G	Avulsion channels that feed sand paludally onto the floodplain; predominantly oblique to main paleoflow (Miall 1996; Bridge 2003).
	Crevasse splay	CS	E, F, K, J, L	Sedimentary waning-flow sand sheets over the floodplain after a breach of levee (Reineck and Singh 1980; Bridge 2003), sheet-like pulsatory deposition on the floodplain (Makaske 2001; Slingerland and Smith 2004)
	Floodplain	FF	L, K ,J	Extensive, thick mudstones/siltstones; pedogenic soil horizons. Anastomosing system dominant background deposition suggests long floodplain residence and avulsion stratigraphy (Makaske 2001; Miall 2016).

Table 2. Architectural elements identified in the Gercus formation in the Merade and Khalakan sections.

coinciding adjacent to CH, SB, CC, and CS elements, which fine and thin away from the channel margin (Miall 2016). Levee elements are wedge-shaped to lenticular, elongate in cross-section, and lie parallel to the channel axis (Text-fig. 8A). In the same section, the levee element reaches about 2 m in thickness.

Crevasse Channel (CC): Predominantly composed of facies (A, D, E), featured by ribbon-like bodies, internal scours, and an erosional base. Lag deposits are often situated at the base, containing fossil remains such as petrified plants. This element shows a fining upward trend, architecturally situated adjacent to LV and CS and bounded by FF elements (Miall, 2016), and branches out from the main channel (CH) (Makaske 2001; Miall 2016). The CC element is widely observed in both sections (Text-fig. 8A, Ā).

Crevasse Splays (CS): Principally incorporating facies (E, K, and F), with subordinate (J and L) facies, these show thin bedding, a sharp erosional base, and grade laterally and vertically within extensive floodplain FF sediments. The Crevasse Splays element may be distinguished from levee elements LV by their coarse-sized grains, small-scale erosive surfaces, and being independently interbedded in floodplain sediments. This element is laterally continuous, with an overall upward-fining trend. This element is architecturally linked to crevasse channel CC, levee LV, and overlaid by floodplain FF. Crevasse splays are commonly found in both sections; the thickest beds reached 2 m (Text-fig. 8A, Ā).

Floodplain Element (FF): Mainly represented by the extensive flat-lying sheets of fine-grained facies (L, K), with subordinate facies (J), and considered to be the most common element across the sediments in the studied sections. This element is characterized by reddish-brown fine-grained siliciclastic, palaeosol features, pedogenic processes, whitish calcareous sediments, oxidation mottles, root traces and desiccation cracks interbedded together across the overbank. This reflects alternating periods of flooding, drying, and pedogenesis (Tooth 2013). The Floodplain element encloses CH, LV, CC, and CS elements, vertically aggraded and laterally continuous (Makaske 2001; Miall 2016). This element occasionally reaches 15 m in thickness (Text-figs 6 and 8A, Ā, B, B̄).

PETROGRAPHIC ANALYSIS

The terrigenous siliciclastic succession of the Gercus Formation is made up of mudstone, siltstone, sandstone, and polymictic conglomerate horizons. The petrographic analysis of the sandstone lithofacies, involving polarized light microscopy, was carried out not only to quantify the framework grain composition of the grains but also to evaluate the textural characteristics.

Framework grain composition of sandy rocks

Diagnosis of the compositional features of the sandstones provides indications of provenance and tectonic setting. Petrographic analysis was executed on the sandstone and silty sandstone intervals that were suitable for thin section preparation. Point-counting was applied (for 400 points) for each slide to quantitative modal analysis with area-counting techniques (Table 3).

Compositions	Rock type	Detrital grains			Matrix and cement			Micas	Heavy minerals	Pore space	Others	Average 100%
Samples	Rock type	Q	F	L	Carbonate cement	Silica cement	Clay minerals					
MG13	pebbly sandstone	17	4	47	9	2	13	4	2	2	1	100
MG19	sandstone	14	3	51	5	2	19	5	1	1	0	100
MG21	sandstone	10	5	34	23	3	15	3	3	1	4	100
MG31	pebbly sandstone	19	4	51	8	2	8	3	1	2	3	100
MG39	sandstone	15	3	39	11	3	11	6	2	8	4	100
MG40	sandstone	8	3	58	11	10	6	3	2	1	0	100
MG44	pebbly sandstone	11	5	45	13	5	12	3	2	4	2	100
MG50	pebbly sandstone	7	3	46	15	3	10	5	2	7	2	100
MG56	sandstone	15	5	48	11	5	9	2	2	2	1	100
MG58	sandstone	14	6	50	12	5	4	4	3	2	1	100
KhG19	sandstone	11	5	48	14	4	9	2	4	2	2	100
KhG28	sandstone	9	3	60	6	3	4	5	5	6	1	100
KhG35	sandstone	15	6	53	11	2	2	4	2	2	3	100
KhG39	sandy siltstone	6	2	20	19	9	33	3	2	4	5	100
KhG40	sandy siltstone	5	0	32	14	3	33	4	1	4	5	100
Ave.%	average	12.3	3.6	45	12.3	3.5	13.4	3.5	1.8	3.0	2.4	100%

Table 3. Percentage ratio of QFL compositions in the selected thin sections of the Merade and Khalakan sections. Note: MG19, MG21, KhG39, and KhG40 represent the lithic wacke; while the remaining samples represent lithic arenite.

At the Merade section, petrographic examination of the slides reveals that lithic fragments are the main framework component, outnumbering quartz and feldspar; feldspar is subordinate to quartz. Quartz grains are characterized as monocrystalline, with some polycrystalline ones. Furthermore, they vary from angular to subrounded and from fine-to-coarse in size. The lithic fragments are compositionally heterogeneous, but the majority of them are sedimentary rock fragments, chert, and carbonate; others are metamorphic and volcanic clasts, and they are associated with muscovite, biotite, heavy minerals, and organic matter in varying amounts (Text-fig. 9A, B). Feldspar is the least common framework element in the samples examined and includes altered feldspar, as well as plagioclase and K-feldspar. Diagenetic cements comprised clay and carbonate matrix, with minimal authigenic quartz in settings characterized by syntaxial overgrowth on detrital quartz grains.

The Khalakan section shows a different petrographic composition, where there has developed a dominance of fine-grained clastic sediments that contain an elevated abundance of carbonate-rich detritus. The basic parameters of the sandstone and siltstone as determined from thin section analysis reveal relatively high quartz content and moderate lithic fragment abundance with subordinate feldspar.

The quartz grains are exceptionally monocrystalline with minor polycrystalline types, with subrounded to angular morphologies. Meanwhile, the lithic fragments comprise clasts of fine-grained volcanic, metamorphic, and sedimentary source rocks, dark grey-brown carbonaceous clasts (Text-fig. 9A, B), and varying amounts of muscovite, heavy minerals, and brown plant tissue fragments. Feldspar is particularly scarce and occurs as cloudy subhedral albite and alkali feldspar grains (Table 3).

Cements and clay minerals are common in siltstone horizons within the Khalakan section, constituting ~25% of thin-section area. Clay minerals that have a brown color in PPL and show low-to-moderate birefringence in XPL are present as finely disseminated matrix material that fills intergranular pore spaces (Text-fig. 9C, D). Carbonate cements are a significant matrix constituent of siltstone and calcareous siltstone lithofacies. This cement, which ranges in size from fine to medium crystalline, occludes porosity and shows bright to orange interference colors in XPL. Silica cement is minimal, occurring as sparse quartz overgrowths that are sometimes indistinguishable from detrital quartz and is absent from some samples. Calcareous silty thin sections contain diverse microstructures, such as fine-crystalline micrite and iron staining, and floating detrital grains. Fractures and voids contain micrite with the vug occupied by sparry calcite and clays (Text-fig. 9E, F).

The sediment succession of the Gercus Formation underwent modification subsequent to deposition and burial. The progress of diagenesis can be reconstructed through the three well-distinguished stages of diagenetic alteration proposed by Choquette and Pray (1970). These include eogenesis, connected with shallow burial, Mesogenesis, associated with deep burial at high temperature and pressure; and

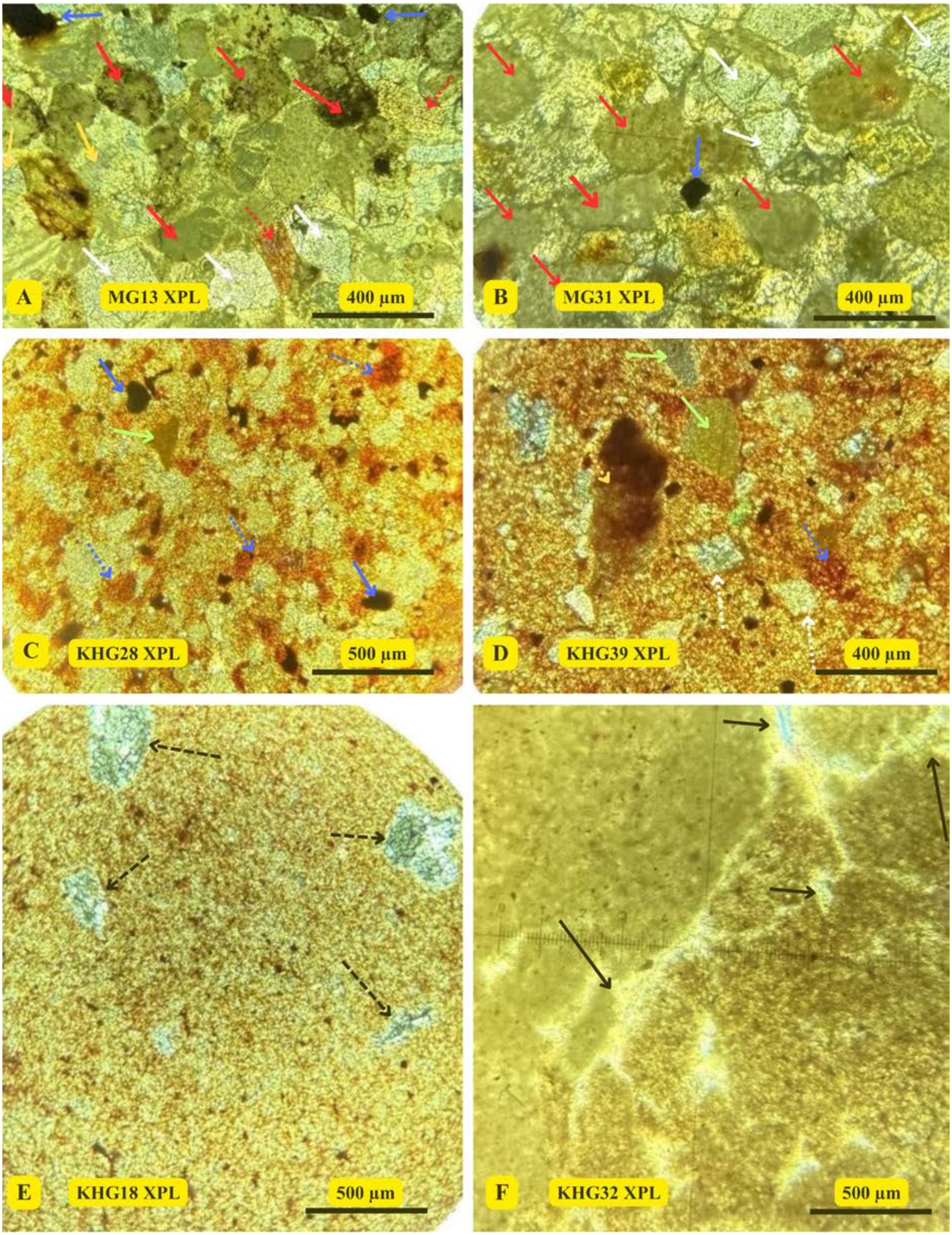

Text-fig. 9. Petrography Photomicrographs of Gercus sandstones and sandy siltstones representing their components, taken under cross-polarized light (XPL). Quartz: white arrows; Feldspars: yellow arrows; Lithic Fragments: red arrows; Chert: green arrows; Clay Minerals: blue dotted arrows; Carbonate: yellow dotted arrows; Micas: red dotted arrows; Dolomite: white dotted arrows; Iron Oxide: blue arrows; Detrital Floating Grains: black dotted arrows, and Sparry Calcite filling vugs and Fractures: black arrows.

Telogenesis, connected with uplift or following uplift (Boggs 2009). Mechanical compaction is clearly apparent in closely packed sand grains, oriented mica flakes, and reduced pore space. Red staining from iron oxides (hematite/goethite) is observed through the grain coating, implying oxidizing conditions, which typically take place during the early diagenetic stage or shortly post deposition (Collinson *et al.* 2006). Cementation is also observed; many zones of carbonate cement can be seen, particularly in the calcareous fine sediments, commonly binding grains, indicative of meteoric phreatic conditions or groundwater fluctuations, and it may occur early or through mesogenesis stages (Boggs 2009; Tucker 2023). The authigenic clay minerals filling pores and lining grain boundaries are evidence of diagenetic modification from feldspar and lithic fragment alteration at early to intermediate burial depths. This process is often associated with the in-situ dissolution of unstable detrital components and the subsequent precipitation of kaolinite, chlorite, or illite (Ajdukiewicz and Lander 2010).

A low ratio of silica cement would also indicate little quartz overgrowth and that the sediments did not attain high enough thermal or pressure maturities required for extensive quartz precipitation (Henares *et al.* 2020). Minor scattered dark opaque organic matter suggests the presence of remnants of terrestrial plant debris with iron oxides, hinting at an early diagenetic stage and oxidation. These conditions assist the precipitation of iron-rich minerals such as hematite in the shallow burial stages (Schmid *et al.* 2004).

The diagnostic constraints on source-rock lithology and tectonic setting are afforded by the detrital grain composition in stratigraphic rocks. The petrographic results for the compositional analysis of the sandstone beds shows that the lithic fragments are more than feldspar and quartz and have textural immaturity characteristics (Table 3). This shows that the litharenite is predominant, while only four samples (MG19, MG21, KHG39, and KHG40) are considered lithic wackes (matrix ≥ 15%) which is achieved by Folk's (1974) ternary diagram, (Text-fig. 10A). The high quantity of monocrystalline relative to polycrystalline quartz implies plutonic-dominated provenance over a metamorphic source (Text-fig. 10B).

Based on established provenance discrimination frameworks that consider litho-detritologic composition in relation to tectonic setting (Dickinson and Gehrels 2009; Weltje and von Eynatten 2004; Garzanti *et al.* 2007), the detrital mineralogical signatures of the investigated stratigraphy point to derivation from recycled-orogenic environments, magmatic arc terranes, and foreland uplift sources (Text-fig. 10B), consistent with the established discrimination criteria for convergent margin provenance (Garzanti 2016; Marsaglia and Ingersoll 2018; Caracciolo 2020).

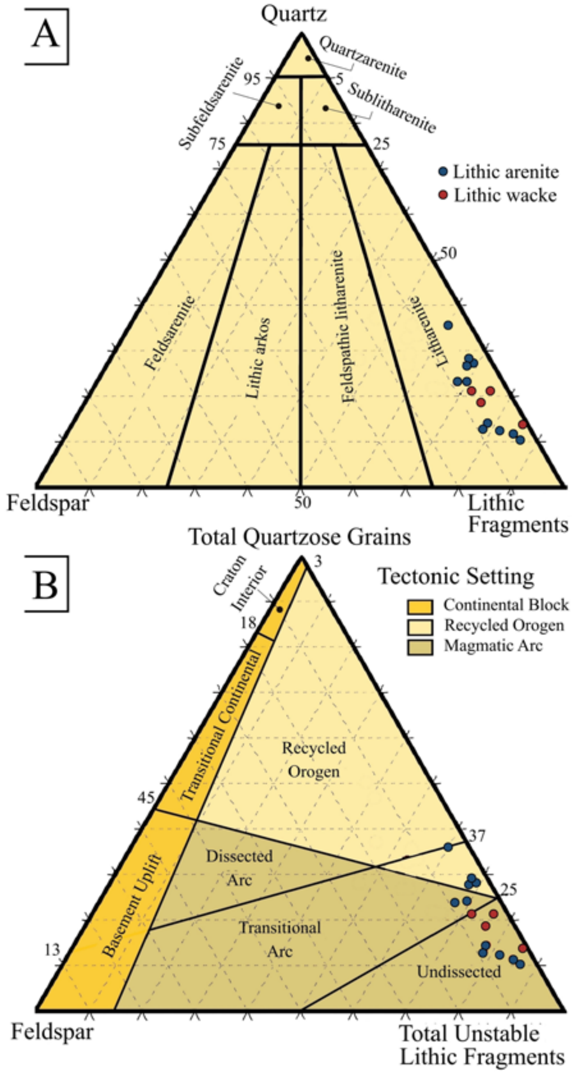

Text-fig. 10. Triplot of A) QFL classification by Folk (1974), using count data of sandstone and siltstone beds as indicated in Table 3. B) Relationship between tectonic setting and framework composition provenance (Dickinson *et al.* 1983).

MINERALOGICAL ANALYSIS

The techniques used in the mineralogical analysis include the X-ray diffraction (XRD) technique, which applied for the fine-grained bulk geochemical analysis of the fractions and also used for clay mineral assemblage determination and clay classification.

Mineralogical composition of fine-grained rocks

The mineralogical composition of the fine fraction (<62 µm) was studied by X-ray diffraction (XRD) analysis. The mineralogical results (Table 4; Text-fig. 11) indicate the dominant presence of dolomite, quartz, palygorskite, and a minor proportion of calcite, chlorite, hematite, and graphite-forming assemblage. The mineralogical association presents agreement with previous studies carried out in the area by Al-Rawi (1983), Dhannoun *et al.* (1988), and Kettanah *et al.* (2020). Diagenetic dolomitization usually takes place by means of reaction between Mg-rich fluids and earlier carbonate phases, with calcite dissolution and clay minerals being replaced incrementally (Morad *et al.* 2012; Warren 2000). Alternatively, detrital dolomite could be sourced from the carbonate-dominant source terrains in the catchment area (Machel 2004).

Detrital quartz is the most stable and makes up to about 19% of the total mineral assemblage in the siliciclastics. Despite not being the predominant component, it is consistently present, indicating a continuing influx of terrestrial detritus (Milliken and Mack 2003; Potter *et al.* 2004). The stability of quartz during sediment transport and diagenesis makes this mineral an excellent indicator of provenance (Weltje and von Eynatten 2004). Palygorskite is the third most abundance component, and it is also a fibrous magnesium-aluminum phyllosilicate. This mineral generally grows in authigenic mode under semi-arid/arid climatic conditions with high evaporation rates and alkaline pH (Galán and Singer 2011; Kehl *et al.* 2021; Singer 1989). Its occurrence indicates episodic palaeosol processes or early diagenetic provenance in restricted freshwater (lacustrine and floodplains) to marginal marine environments (Weaver and Beck 1977).

Accessory minerals are chlorite (4.8%), calcite (4.5%), hematite (3.85%), and graphite (3.2%). Chlorite is a product of mechanical weathering in low- to medium-grade metamorphic terranes or source rocks that are mafic igneous in nature (Hillier 1995; Velde 1995). Chlorite may also form authigenically with burial diagenesis, replacing ferro-magnesian silicates (e.g., biotite, pyroxene, and amphibole) or unstable volcanic lithic fragments (Jahren and Aagaard 1989; Worden and Morad 2003).

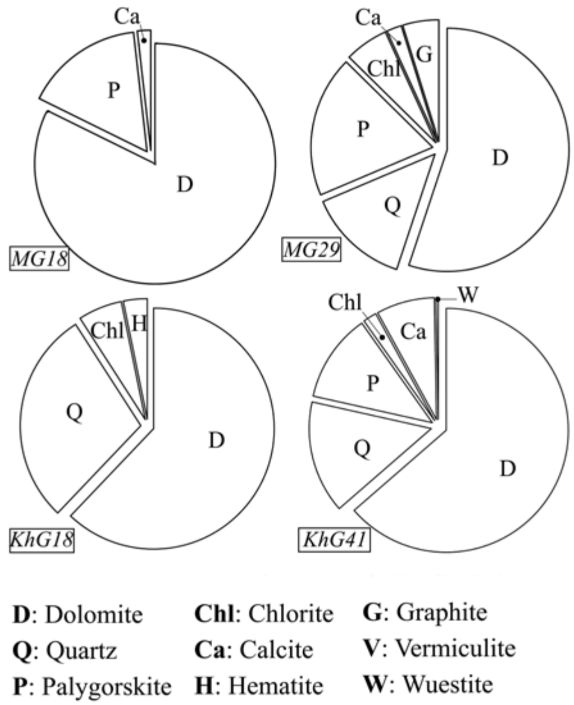

Text-fig. 11. Percentage value of mineral constituent of muddy-sized fractions tested by XRD technique.

Calcite is present in minor amounts and was possibly sourced partly as detrital grains transported from carbonate platforms (Tucker and Wright 2009) or as an authigenic precipitate under shallow burial diagenetic conditions. Calcite cementation is generally established at the meteoric phreatic-marine pore waters interface where precipitation due to supersaturation takes place (Morad 1998; Bjørlykke 2014). Hematite is confined in the Khalakan section and usually occurs as a result of oxidative weathering of the source Fe-bearing minerals, such as magnetite, siderite, ferrous chlorite, etc., under oxic-like

Minerals/ Samples	Rock type	Bed thickness (M)	Dolomite	Quartz	Palygorskite	Chlorite	Calcite	Hematite	Graphite	Wuestite	Total %
MG18	mudstone	12	82.3		15.9		1.8				100%
MG29	mudstone\siltstone	11	55.1	13.5	18.8	5.8	2		4.8		100%
KhG18	mudstone	2.8	62.1	28.8		5.9		3.2			100%
KhG41	shale	0.5	63.6	14.9	11.7	1.8	7.7			0.3	100%

Table 4. Percentage mineralogical compositions of reddish-brown and fine-sized fractions conducted by XRD test.

diagenetic conditions (Liu *et al.* 2019; Cornell and Schwertmann 2003). Its presence, restricted to a particular area, could indicate spatial heterogeneity in local redox or differences in detrital assemblages.

Graphite is a stable carbon polymorph, found uniquely in the Merade section that might have originated from graphitic carbonaceous shales (Luque *et al.* 2014; Beyssac and Rumble 2014). Graphitization typically occurs in carbonate-clay sediments that were heated to high temperatures and experienced long periods of fluid-rock interaction during metamorphism or deep-burial diagenesis (Beyssac *et al.* 2002; Buseck and Beyssac 2014).

Clay minerals

X-ray diffraction indicates that the clay mineral assemblage predominantly consists of illite and chlorite, accompanied by subordinate kaolinite, palygorskite, and mixed-layer kaolinite-chlorites (Text-fig. 12). Diffraction patterns of the sample (KhG16) at 14.2 Å, 10.0 Å, and 7.1 Å are more intense than those that are assigned to chlorite, illite, and kaolinite-chlorite mixed layers. After treatment with ethylene glycol, the presence of a new peak around 10.5 Å is characteristic for palygorskite, and the maintenance of stability of the 14 Å reflection after heating at 550°C confirms that the chlorite is not expandable and thermally stable. The illite peaks that remained after glycolation and heating also indicate a well-ordered dioctahedral mica-type structure, characteristic of a burial diagenesis (Moore and Reynolds 1997; Środoń *et al.* 2014).

As a relatively uncomplicated mineral assemblage, the dominant minerals of sample (KhG36) are illite and kaolinite with strong peaks at 10 Å and 7 Å; no distinct peak is observed at 14 Å (the exclusion of chlorite), and the retention of kaolinite peaks in X-ray patterns even after heating to 550°C indicates that the lower Fe content gave fine stability to the Al-rich constituents (Wilson 2013). This diagenetic association could represent a weathering of acid continental environments or hydrolytic transformation at shallow burial (Chamley 1989).

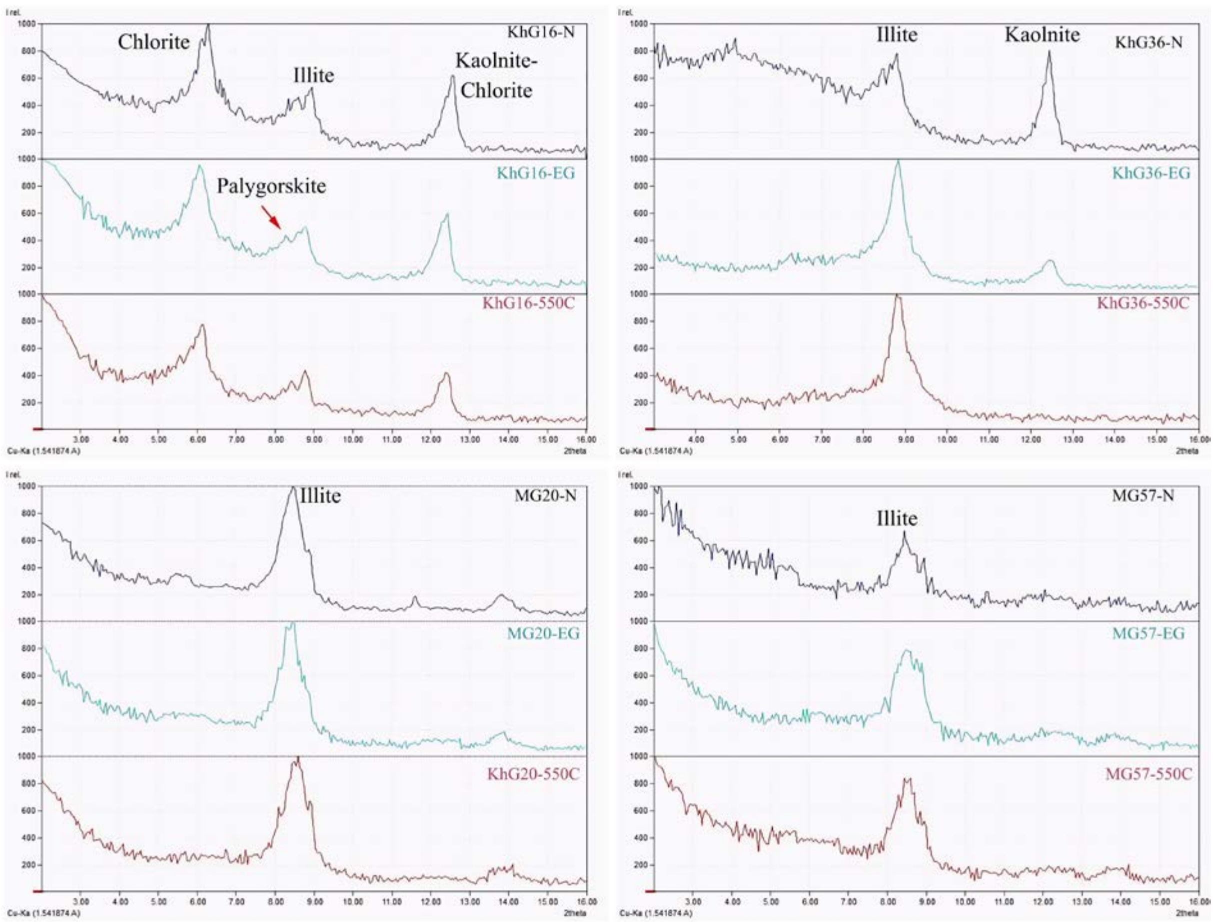

Text-fig. 12. Stacked X-ray diffraction (XRD) patterns of oriented clay-size fractions (Sample codes are placed with the plots).

In samples MG20 and MG57, the patterns exhibit a single dominant illite reflection at 10 Å under all treatments (N, EG, and 550°C), which shows that the clays are predominantly composed of illite with small amounts of kaolinite. The lack of expandable smectitic or mixed-layer phases indicates moderate to advanced diagenetic maturity, generally reflecting burial beyond 2–3 km and temperatures over ≈100°C, above which illitization reactions usually prevail (Środoń *et al.* 2014; Berger *et al.* 2020). The uniformity of these illite-rich textures testifies to an advanced (smectite) illitization and recrystallization under long-term, low-permeability conditions (Ylagan *et al.* 2000).

In general, the clay mineral assemblages indicate a mixed detrital-diagenetic provenance. The predominance of illite and chlorite indicates a provenance from metamorphic and volcanic source terrains, whereas the minor contents of kaolinite and the palygorskite fraction reflect processes of subaerial exposure, oxidative pedogenesis, and semi-arid depositional conditions. The presence of illite and chlorite following heating reveals that the clay assemblages were thermally stable to a diagenetically mature state, thus interpreting moderate burial and little to no chemical transformation of the sedimentary system (Singer 2002; Wilson 2013).

DISCUSSION

Depositional environment

The studied sections are characterized by six architectural elements (CH, SB, LV, CC, CS and FF) (Table 1; Text-figs 6 and 8). The proportion of each element was calculated by the thickness ratio with respect to total section thickness (Text-fig. 8C). Channel fills and overbank components account for ~9% and 91%, respectively, of the total thickness as represented by the modeled average profile. Channel-fills CH are often repeated in the Merade section, sometimes within floodplain sediments surrounding them, and may be stacked vertically; thus they account for 11.2% (Merade section) and 2.7% (Khalakan section) of total thickness. Vertical accretion of the SB element occurs less in the channel-fill elements (around 1% and 2.3%, respectively, at Merade and Khalakan sections), however, CH being dominant over the SB element. Nevertheless, erosive surfaces within the fills are well preserved (Text-fig. 8A, Ā).

Among the elements of overbank deposits, FF is the predominant element in the sections. This indicates that the depositional environment of the selected sections was characterized by a floodplain development. In addition, crevasse splay (CS) accounts for a large proportion of floodplain successions as well, occupying 5.4 and 13.1% in the Merade and Khalakan sections, respectively. Crevassing was probably the predominant aggradational process on the floodplain.

Based on the fluvial facies type models, which were introduced by Miall (2016), an anastomosing fluvial system appears to be the most compatible with the sedimentary features of the studied sections. (Text-fig. 13) displays a generalized model of the depositional environment of the studied sections. An anastomosing river system is a multi-channel network that consists of interconnected, laterally stable channels that enclose floodplain islands and it basically evolves through vertical accretion and avulsion under low stream power conditions, cohesive banks, and sustained fine-grained sedimentation (Schumm 1968; Smith and Smith 1980; Makaske 2001; Tabor and Myers 2015; Miall 1996, 2016).

Crevasse channels and crevasse splays are commonly prominent elements in the anastomosing fluvial system, where channel response is dominated by crevassing processes and transition to stable crevasse channels (Smith *et al.* 1989; Nanson 2013; Miall 2016). Crevasse channel flow may subsequently reenter the main channel downstream or be diverted into the paleochannel course, which generates the large divergent flows (Smith 1983; Smith *et al.* 1989).

The current study's architecture elements provide the most internally consistent quantitatively constrained interpretation, rather than either a delta or distal fan settings (Ameen, 2006; Karim *et al.* 2018), whilst an interaction with aeolian settings might be possible (Maroulis *et al.* 2007). The six architectural elements identified here are basically irreconcilable with an alluvial fan model, which would be predicted to require a greater percentage of high-energy, coarse-grained AEs, and a less laterally extensive floodplain than is the case. The prevalence of Floodplain fines (FF) and the considerable contribution of Crevasse-splay deposits (CS) in the studied sections is a diagnostic signature of a high aggradation rate, giving the features seen in the present system – a high amount of suspended sediment, a cohesive flood plain, low-gradient, and a multi-channel fluvial system (Makaske 2001; Makaske 2017). The vertical and spatial arrangement of the channel-fill components occur in a much lower proportion than would be expected for a sheet flood-fed alluvial fan, which would have given characteristically narrow, stable anastomosed channels confined to low energy floodplain surfaces (Text-fig. 8A, B).

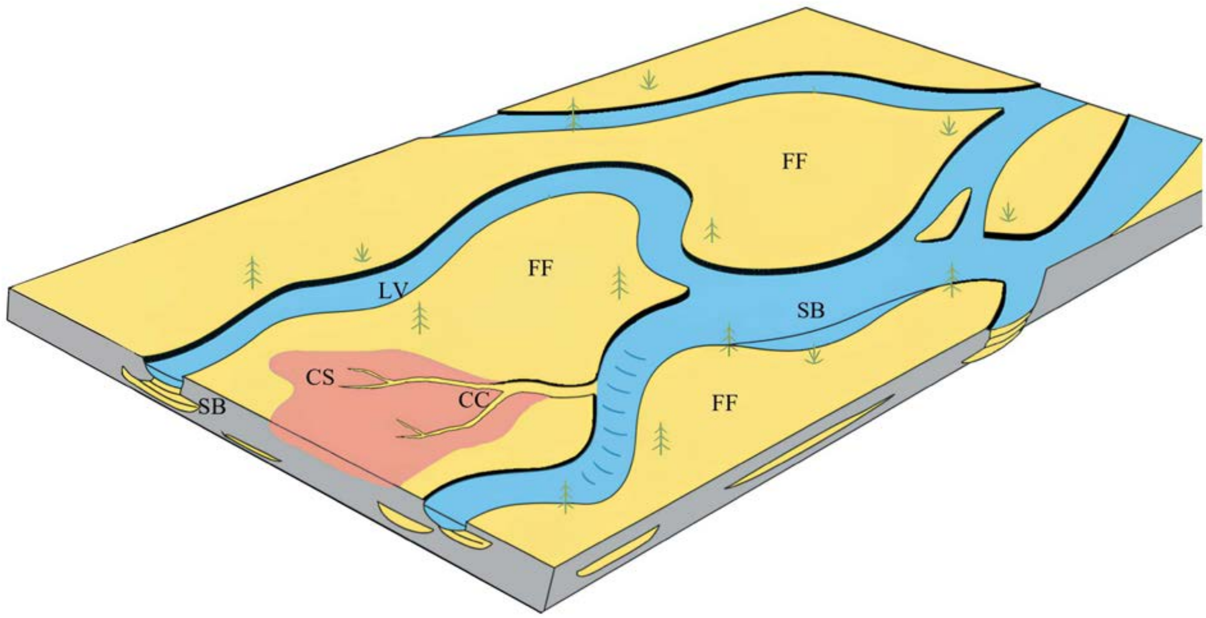

Text-fig. 13. Depositional environments of anastomosing fluvial system, proposed for the studied sections of the Gercus Formation, shows the distribution of the architectural element deposits. Modified after Miall (2016). CH: channel fill, SB: sandy bedform, LV: Levee, CC: crevasse channel, CS: crevasse splay, FF: floodplain.

Anastomosed fluvial systems exist in different environments from humid to arid climates and have a low gradient river as the primary internal control factor, which is closely related to tectonism and rapid subsidence (Miall 2016). It has been interpreted that such river systems are developed when the river underflows a rapidly subsiding basin and is tectonically actively controlled, though a downstream damming effect influenced by the localized bedrock condition (Makaske 2001; Miall 2016).

Looking across the regional exposures of the Gercus Formation, it is interpreted herein as a syntectonic molasses-type succession that accumulated in an active subsiding foreland basin closely related to the building of the Zagros orogenic deformation and Neo-Tethyan closure during Mid-Eocene time (Numan 1997; Jassim and Goff 2006; Aqrawi *et al.* 2010; Hussain and Aghwan 2014; Karim *et al.* 2020).

The Cooper Creek anastomosing river system, central Australia, remarkably bears a strong correspondence with the system interpreted for the current successions, so that this is likely a convincing and relevant active modern analogue for reconstructing both the palaeoclimate and depositional environment conditions of the Gercus Formation (Nanson *et al.* 1986; Knighton and Nanson 1994a; Knighton and Nanson 1994b; Maroulis *et al.* 2007).

Provenance and tectonic setting implications

The petrographic results of the Gercus sandstones reveal a lithic-rich framework grain composition that is compatible with their classification as a litharenite. This has been similarly documented by Malak *et al.* (2019) and Kettanah *et al.* (2020). Modal QFL analysis from the current investigation shows that lithic fragments make up 74% of the framework grains, while subordinate quartz and feldspar level up the remaining portion with 20% and 6%, respectively. Recalculating on the clay matrix basis, the majority of the studied samples are classified as lithic arenites, whilst certain sandstone samples (MG19, MG21, KHG39, and KHG40) (Table 3; Text-fig. 10A) are classified as lithic wackes, reflecting elevated clay contents (15–33%). The overall textural immaturity of the framework grains with their irregular to subangular grain forms, as well as the polymictic and diverse lithic assemblages, suggests short transport distances during deposition close to the source terrane, which consisted of a sedimentary or low-grade metamorphic source, from which there was derived a substantial variety of sedimentary-volcanic-plutonic-metamorphic rock fragments (Kettanah and Bamarni 2018). The total petrographic characteristics paired with the compositional immaturity point to derivation from a heterogeneous geological source terrane and an active tectonic terrane.

The presence of carbonate and chert lithics compiled with other provenance features essentially indicates recycling from pre-existing deposits, most probably the Cretaceous carbonate and radiolarian chert successions found in the Imbricated and Suture Zones of northeastern Iraq, particularly the Balambo and Qulqula Radiolarian Formations (Kettanah *et al.* 2020).

The diverse heavy mineral assemblages identified in the Gercus Formation, especially the opaque phases – chiefly chromian spinel, magnetite, ilmenite and hematite which have been found to be the dominant heavy mineral constituent (Kettanah *et al.* 2020; Aziz *et al.* 2021; Nasif and Khwedim 2022; Al-Jubory *et al.* 2023), all can be consistently sourced to the basic and ultrabasic parent lithologies of the Zagros ophiolitic complexes. The non-opaque fraction, and the ZTR group (zircon, tourmaline and rutile) together with the epidote-group minerals, garnets and amphiboles give confirmation of a secondary input from recycled sediments and medium-grade metamorphic terranes. Al-Jubory *et al.* (2023) using EPMA to show that the detrital chromites belong to the Al-chromite group with high Cr values (0.4–0.87), low TiO_2 contents, consistently plotting in the field of supra-subduction zone fore-arc peridotites, confirming their derivation from harzburgitic ophiolite. The heavy mineral investigations combined with geochemical data reinforces the conclusion that the Gercus Formation derived its provenance from and was displaced into an eroding Zagros-Taurus ophiolitic and metamorphic nappe system during final closure of the Neo-Tethys Ocean.

The total petrographic, heavy mineral, geochemical and geochronological data given above provide a coherent tectonic provenance model for the Gercus Formation. The elevated lithic content, compositional and textural immaturity, dominance of carbonate and chert rock fragments, small amount of mafic-metamorphic lithics and high chromian spinel abundances provide a collective indicator for deposition in a foreland basin that received detritus from an actively eroding collisional orogen. The source terrane consists of two major components: (A) recycled sedimentary sequences (chert rich and carbonate dominated such as the Qulqula Radiolarian Formation and the Balambo Formation), the former deposit having accumulated in the Zagros Fold-Thrust Belt (ZFTB), (B) ophiolitic complexes within the igneous-metamorphic rocks of the Zagros Suture Zone (ZSZ), represented by the Penjween-Walash terrane including its counterparts in northwestern Iran and southeastern Turkey.

The fore-arc to supra-subduction zone signature of detrital chromites (Al-Jubory *et al.* 2023), the occurrence of subduction-diagnostic glaucophane (Kettanah *et al.* 2020; Nasif and Khwedim 2022) and the Albian–Cenomanian magmatic arc zircon ages (Aziz *et al.* 2021) are mutually consistent with a tectonic scenario in which the sediments of the Gercus Formation were deposited as part of a flysch-to-molasse transition sequence in a flexural foreland basin that developed outboard of an advancing ophiolitic nappe stack during final-stage Neo-Tethyan subduction followed by incipient Arabian-Eurasian collision. This interpretation is consistent with the wider regional framework proposed for the Middle Eocene stratigraphy of the Zagros Fold-Thrust Belt in which the Gercus Formation represents a late stage of molasse that overlies the Maastrichtian–Middle Eocene foreland cycle. (Aziz *et al.* 2021).

Mineralogical assemblages and paleoenvironmental implications

Mineralogical X-ray diffraction analysis of four representative samples from floodplain finestone facies MG18, MG29, KhG18, and KhG41 (Table 4), reveals that dolomite, quartz, and palygorskite are the basic mineral assemblages, with minor amounts of calcite, chlorite, hematite, and graphite, as shown in (Text-fig. 11). These mineralogical components are consistent with assemblages reported from correlative deposits in NE Iraq, as previously recorded by Dhannoun *et al.* (1988).

The third most abundant mineral phase, palygorskite, plays an essential role in paleoclimatic reconstruction. Authigenic palygorskite develops under arid to semi-arid stages with high Mg/Ca ratios and relatively higher pH levels (>8) (Singer 1989; Jones and Galán 2008). However, the association of palygorskite with dolomite (MG29, MG18, KHG41) is a characteristic of alkali, evaporitic lakes, playa-mudflat or poorly drained floodplains (Millot 1970; Weaver and Beck 1977; Środon *et al.* 2014), under what is primarily a seasonally arid environment but may nevertheless be a seasonally semi-wet/dry climate.

The most potential Mg/Ca enrichment scenario is given by MG18, with 82.3% dolomite, 15.9% palygorskite, with minor calcite 1.8%, (Table 4). Nearly-absence of calcite coupled with high dolomite may indicate late-stage Ca-drawdown that is potentially reconcilable with biological activities having out-competed and thus exhausted dissolved Ca preferentially into biological carbonate, resulting in Mg-enriched residual waters (Środon *et al.* 2014). MG29 and KHG41 preserve calcite with dolomite and Palygorskite as mentioned suggesting intermediate evaporative stages when Ca was not yet fully sequestered, possibly representing proximal or earlier phase equivalents of MG18.

Most noticeable is the 4.8% graphite presence in MG29 (Text-fig. 11), and this will be discussed later. The carbonaceous material of graphite represents thermally altered organic matter which normally indicates burial metamorphism or hydrothermal overprint. However, its presence should be considered in order to determine if the assemblage is representative of a high-organic-input facies that was then altered.

In contrast, the Hematite, substantially observed in KHG18, shows oxidizing, subaerial conditions. It is dolomite-dominated, with higher quartz, and no palygorskite (KHG18; Table 4). The absence of palygorskite coupled with the presence of hematite suggests a drier, more oxidizing period, perhaps a soil horizon or exposure of a floodplain surface, where the water table fell and evaporative Mg/Ca enrichment did not reach sufficient levels for palygorskite to occur, or whatever palygorskite had formed was later destroyed by oxidizing diagenesis.

In need of explanation is the (MG/KHG) specimens' studied dichotomy containing palygorskite co-occurring with dolomite in addition to hematite, when it has been noted that palygorskite and hematite should not occur together, being indicators of ephemeral lake versus subaerial oxidizing soil conditions (Środon *et al.* 2014). This implies that we have here characteristics of alkaline evaporitic lakes, playa-mudflat or poorly-drained floodplains and palaeosols (Millot 1970; Weaver and Beck 1977; Środon *et al.* 2014), under a surface that is mostly seasonally arid to semi-arid climate conditions.

Lateral facies variations and redox conditions

The prominent mineralogical differences between the studied sections, which are inferred from the studied mineral compositions, can be related to distinct lateral facies variations and paleoredox conditions. Graphite is only present as a surface concentration in the Merade section, while the Khalakan section is the only section that has hematite. Although the concentrations of these minerals are within trace amounts, they are critical mineralogical indicators of differing depositional and diagenetic redox environments.

Graphite can form or be preserved under reduced conditions during sedimentation or early diagenesis (Luque *et al.* 1998). The occurrence of graphite in the Merade section implies a relatively deeper environment with reduced energy and consistent organic matter accumulations and decomposition, limited pore-water movement, and sub- or anoxic bottom waters near depositional sites in topographically lower settings. Conversely, hematite is direct evidence of oxidizing diagenetic conditions (Walker 1967; Turner 1980), which shows well-drained, topographically elevated floodplain environments with oxic pore-waters and atmospheric exposure in drying conditions. The presence of hematite in the Khalakan section could mean that ferruginous paleosol occurred under semi-arid, seasonal wetness in an area with fluctuating water tables. We can infer that these mineralogical distinctions depict lateral changes from a poorly drained, floodbasin environment in the Merade section to a well-drained levee or interchannel floodplain setting.

Paleoclimatic interpretation of clay assemblages

X-ray diffraction analysis, as shown in (Text-fig. 12), has uncovered differentiated clay mineral assemblages representing different depositional conditions and diagenetic pathways. Sample KhG16 disclosed an illite-chlorite-dominated assemblage with subordinate kaolinite, palygorskite, and mixed-layer phases. The KhG36 sample was characterized by samples of illite and kaolinite associations lacking chlorite. Illite is the dominant mineral in samples MG20 and MG57; kaolinite occurs in minor quantities, signifying relatively high maturity of diagenesis.

The illite-chlorite dominance in KhG16 and the illite-rich character of MG20/MG57 attribute derivation from physically weathered source rocks formed under cool to temperate, low-humidity conditions with limited chemical weathering (Chamley 1989; Thiry 2000). The presence of kaolinite in KhG36 indicates episodes of enhanced chemical weathering in the source area under warm, humid conditions with adequate drainage (Chamley 1989; Thiry 2000; Wilson 2013; Dill 2020). The presence of palygorskite in KhG16 indicates arid to semi-arid paleoclimatic conditions (Singer 1989; Galán and Pozo 2011). Palygorskite forms authigenically in alkaline, Mg-rich water bodies with restricted drainage and high evaporation rates (Singer 2002). Its association with kaolinite in KhG16 indicates climatic oscillations between humid conditions during enhanced chemical weathering and semi-arid conditions (Thiry and Jacquin 1993).

Clay minerals can be used as burial diagenesis and thermal history indicators. KhG16 displays moderate burial diagenesis at a burial depth of 1–2 km and temperature of 60–100°C, which is characterized by well-ordered illite and thermally stable chlorite, intermediate-breaking mixed-layer phases (Jahren and Aagaard 1989). KhG36 reflects shallow burial diagenesis at a burial depth of <1 km and temperature of <60°C, which is manifested in the preserved detrital texture and low transformation of the clay minerals (Chamley 1989; Wilson 2013). MG20 and MG57 show advanced diagenesis with complete illitization at a burial of more than 3 km and a temperature of 120–150°C, a result of burial diagenesis and subsequent annealing under low-permeability conditions (Ylagan *et al.* 2000; Meunier 2005; Środoń *et al.* 2009; Soua 2025).

Thus, the initial deposition of the clay mineral assemblages of the current study took place during variable climatic conditions from arid to semi-wet. The source terrains including metamorphic and igneous rocks, supplied illite and chlorite, the amounts adjusted through physical weathering. Thereafter, progressive burial resulted in differential diagenetic modification, whereby the shallow-buried sediments of KhG36 retained primary mineralogy compared to the deeply buried units of MG20 and MG57 that underwent clay mineral transformation.

Calcareous pedogenic formation implications

Different microstructures caused by pedogenic processes can be seen in the muddy horizons of (FF and CS) elements. They consist of fine-crystal-sized micrite-microsparitic textures and iron staining, floating detrital grains, voids, and cracks (Text-fig. 9E, F). These microstructures are filled by sparry calcite and clays, and may have been formed diagenetically through vadose zone processes (Wright and Tucker 1991; Alonso-Zarza 2003).

Micromorphological characteristics, such as the predominance of micritic groundmass with localized microspar growth and the absence of vadose silt, indicate that the floodplain facies developed during conditions of relatively high but periodically interrupted soil moisture availability (Watts 1980; Khadkikar *et al.* 1998). The existence of the primary sedimentary textures beneath carbonate accumulations indicates that cementation took place after the initial deposition of the sediments, which is generally consistent with syngenetic to early diagenetic levels of carbonate formation driven by pedogenic soil processes rather than reaching deep in the burial diagenesis (Mack *et al.* 2000). This hypothesis was further tested by the lateral consistency and variable thickness of the calcareous horizons that were observed in outcrop, which were most likely subjected to topographic gradients in the pedogenic influence within that floodplain area.

The presence of detrital silicate clasts floating in the micritic groundmass without grain-to-grain contact is diagnostic of calcrete formation, particularly of displacive crystal growth where expanding carbonate cements physically push apart framework grains as precipitation occurs in the vadose zone (Wright 2007). This displacive mechanism of mineral growth is most effective under slow, episodic carbonate infiltration typical of semi-arid pedogenic settings where wetting-front penetration is shallow and evaporative concentration high (Alonso-Zarza 2003).

The preserved macro-pedogenic processes such as; mottles, root traces, carbonate nodules, calcisol development, and desiccation features provide valuable indications. Irregular patches of contrasting coloration mottles, reflecting reduction\oxidized conditions, occur in the floodplain mudrock intervals during water table fluctuations (Kraus 1999). The observed rootlet networks penetrate downwards from distinctive paleosol horizons, providing additional evidence that the coating of pedogenic modification was driven by organic processes and not simply a product of diagenesis. Calcified root tubes, so-called root-induced carbonate rhizoliths, are locally present and register the role of root respiration CO_2 in promoting carbonate dissolution at the rhizosphere then reprecipitation when pore waters migrate down in a vadose zone (Klappa, 1980). Nodular calcareous morphology implies conditions at the drier end of this distribution, generally consistent with semi-arid to seasonally arid planetary scenarios (Royer 1999; Sheldon and Tabor 2009).

The architectural arrangement of these calcareous horizons in overbank deposits is consistent with pedogenic carbonate precipitation, which occurs in conjunction with episodic water table fluctuations and elevated evapotranspiration rates in semi-arid climatic regimes (Kraus and Hasiotis 2006). Such conditions prevail within anastomosing fluvial systems, where low-gradient channels sustain widespread floodplain submergence, succeeded by extended desiccation periods. These circumstances offer idyllic opportunities for carbonate accumulation, commonly in depths of 0.5 to 2.0 m (Retallack 2001). The medley of carbonate-rich and carbonate-poor sediments in the outcrops and thin sections, as manifested by alternate zones, testifies to heterogeneity in the carbonate dispersal within the matrix and implicates periodic dry\wet cycles in place of sustained aridity.

The combination of field-based observations and petrographic analysis hence unequivocally supports the model of a seasonally fluctuating climate suitable for preserving pedogenic features and which experienced regular aridity altering calcium carbonate concentrations within the upper vadose zone (McCarthy and Plint 1998). Connections of such types between wet and dry zones are typical of areas between humid and arid zones, such as low-gradient floodplains, which include anastomosing river systems and floodplains with some to no river networks, which maintain locations due to periods of high stability where soil development dominates (Kraus and Aslan 1993; Makaske 2001). The presence of pedogenic calcareous sediments in the FF element clearly serves as a dependable paleoclimatic indicator of persistent aridity overlaying moist to semi-arid intervals suitable to support the anastomosing river architecture.

CONCLUSION

Sedimentological, mineralogical and petrographic investigations reveal a complex depositional basin development of the Gercus Formation characterized by fluctuating paleoclimatic conditions associated with tectonic sedimentation. The lithic-dominant framework composition (74% lithic fragments, 20% quartz, 6% feldspar) combined with grain morphologies and low textural maturity are consistent with a source of proximal origin having suffered little recycling and limited chemical weathering. The polymictic composition (sedimentary, volcanic, plutonic, and metamorphic) is indicative of derivation from a tectonically active source terrane that is heterogeneous in provenance – both characteristics of foreland basins with high sediment accumulation rates.

Paleoclimate reconstruction from authigenic mineralogy indicates an intermediate climate state between arid to semi-wet\arid regimes. Palygorskite-dolomite aggregates point to seasonally arid conditions yet with periods of water availability. The distribution of the clay minerals documents a gradual diagenetic evolution and confirms an increasing intensity of diagenesis from shallow to deep buried units; some indicators inherited allochthonous illite-chlorite assemblages resulting from physical weathering of high-grade metamorphic-igneous basement rocks exposed in the orogen's flanks, whilst other indicators were representatives of mineralogical transformation. Lateral mineralogical zonation – hematite enrichment at Khalakan and graphite concentration at Merade – signifies redox-controlled facies transitions from poorly drained floodbasin to well-drained interchannel belt. The calcareous (pedogenic) horizons are present in the floodplain deposits and record varying stages of water table fluctuation and enhanced evapotranspiration under semi-arid climatic conditions, with micritic groundmass and localized microspar growth indicating episodic breaks in soil moisture supply.

Six architectural elements (CH, SB, LV, CC, CS, and FF) are typical characterizations for an anastomosing fluvial system that was dominated by widespread floodplain accretion with crevasse channel and crevasse splay development. This architectural composite, combined with pedogenic calcareous horizons, unambiguously suggests ongoing low-gradient floodplain conditions during seasonally varying arid to semi-arid climate regimes favorable for long-term landscape stability and soil formation.

Acknowledgements

The authors are grateful to the Department of Earth Sciences and Petroleum, College of Science, Salahaddin University-Erbil, the Department of Civil Engineering, Garmian University, in the Iraqi-Kurdistan Region, and also to the Iraqi Ministry of Science and Technology and the Iraqi Ministry of Industry for providing logistic support and necessary laboratory equipment used in thisstudy. We would also like to thank the anonymous reviewers for their valuable comments and suggestions of this manuscript. Their constructive review significantly improved the quality of the paper.

REFERENCES

Ajdukiewicz, J.M. and Lander, R.H. 2010. Sandstone reservoir quality prediction. The state of the art. *AAPG Bulletin*, **94**, 1083–1091.

Akça, E., Aydemir, S., Kadir, S., Eren, M., Zucca, C., Günal, H., Previtali, F., Zdruli, P., Çilek, A., Budak, M., Karakeçe, A., Kapur, S. and FitzPatrick, E. 2018. Calcisols and Leptosols. In: Kapur, S. Akça, E. and Günal, H. (Eds), The Soils of Turkey. World Soils Book Series, 139–167. Springer; Cham.

Ali, A.R., Mohammad, O.A.M. and Ahmed, M.S. 2022. Geochemistry of the Middle Eocene Gercus Sandstone, Shaqlawa Area, Northern Iraq: Implications for Provenance, Tectonic Setting and Paleoweathering. *Iraqi Journal of Science*, **63**, 1606–1626.

Al-Jubory, Z.J., Al-Miamary, F.A., Al-Lhaebi, S.F. and Belkin, H.E. 2023. Geochemistry of Detrital Chromite from Gercus Formation (M. Eocene), Northern Iraq: Implications for the Provenance and Paleotectonic. *Jordan Journal of Earth and Environmental Sciences*, **14**, 126–134.

Al-Juboury, A.I., Al-Taee, N.T. and Malak, Z.A. 2021. Paleoenvironmental conditions during deposition of Kolosh and Gercus formations in northern Iraq as deduced from clay mineral distributions. *Iraqi Journal of Science*, **62**, 4791–4801.

Al-Juboury, A.I., Hussain, S.H., McCann, T. and Aghwan, T.A. 2020. Clay mineral diagenesis and red bed colouration: A SEM study of the Gercus Formation (Middle Eocene), northern Iraq. *Geological Journal, Wiley*, **55**, 7977–7997.

Allen, J.R.L. 1984. Sedimentary Structures: Their Character and Physical Basis. Developments in Sedimentology, 30, 1256 pp. Elsevier; Amsterdam.

Al-Mashaikie, S.Z., Al-Azzawi, A.T. and Kadhum, A.K. 2013. Lithofacies Architecture of the Gercus Formation in Jabal Haibat Sultan, NE Iraq. New Concept of Lithostratigraphy and Depositional Environmental. *Journal of Environment and Earth Science*, **3**, 97–114.

Al-Mashaikie, S.Z. and Mohammed, Y.A. 2017. Anatomy of carbonate breccias, turbidite facies and depositional systems of Gercus formation in Dokan area, northern Iraq, *Iraqi Geological Journal*, **50**, 90–103.

Alonso-Zarza, A.M. 2003. Palaeoenvironmental significance of palustrine carbonates and calcretes in the geological record. *Earth-Science Reviews*, **60**, 261–298.

Al-Qayim, B. and Barzani, A. 2021. Facies and stratigraphic associations of Sinjar and Khurmala Formation, Dohuk Area, Kurdistan Region, Iraq. *Arab Journal Geoscience*, **14**, 165.

Al-Qayim, B., Omer, A. and Hemin, K., 2012. Tectonostratigraphic overview of the Zagros Suture Zone, Kurdistan Region, Northeast Iraq. *GeoArabia*, **17**, 109–156.

Al-Qayim, B.A., Al-Mutwali, M.M. and Nissan, B.Y. 2008. Flysch-Molasse Sediments of the Paleogene Foreland Basin of North Arabia, Shiranish Area, North Iraq. *Iraqi Bulletin of Geology and Mining*, **4**, 1–20.

Al-Qayim, B.A., Al-Mutwali, M.M. and Nissan, B.Y. 2008. Flysch – Molasse Sediments of the Paleogene Foreland Basin of North Arabia, Shiranish Area, North Iraq. *Iraqi Bulletin of Geology and Mining*, **4**, 1–18.

AL-Rawi, Y.A. 1983. Origin of Red Color in the Gercus Formation (Eocene), Northeastern Iraq. *Sedimentary Geology*, **35**, 177–192.

Ameen, B.M. 2006. Sequence Stratigraphy of Gercus Formation (Middle Eocene) in Sulaimaniya Area, Northeastern Iraq. *Iraqi National Journal of Earth Science*, **6**, 23–32.

Aqrawi, A.A.M., Goff, J.C., Horbury, A.D. and Sadooni, F.N. 2010. The Petroleum Geology of Iraq, 424 pp. Scientific Press Ltd.; Beaconsfield.

Awad, K.H. and Alsultan, H.A. 2020. Stratigraphic Analysis of Gercus Formation in Dohuk area, Northern Iraq. *Iraqi Journal of Science*, **61**, 2293–2302.

Aziz, N.R., Sadiq, D.M. and Aswad, K.J. 2021. U-Pb Detrital Zircon Dating of Middle Eocene Clastic Rocks from the Gercus Formation, NE Iraq: New Constraints on Their Provenance, and Tectonic Evolution. *Iraqi Geological Journal*, **54**, 1–15.

Bellen, R.C.V., Dunnington, H.V., Wetzel, R. and Morton, D.M. 1959. Lexique Stratigraphique International, Asie, Fascicule Loa, Iraq, 333 pp. National de Ja Recherche Scientifique Centre; Paris.

Berger, G., Lanson, B., Beaufort, D. and Petit, S. 2020. Diagenetic to metamorphic evolution of clay minerals in sedimentary rocks: from field observation to modeling, 207 pp. Earth-Science Reviews; Amsterdam.

Beyssac, O., Goffé, B., Chopin, C. and Rouzaud, J. N. 2002. Raman spectra of carbonaceous material in metasediments. A new geothermometer. *Journal of Metamorphic Geology*, **20**, 859–871.

Beyssac, O. and Rumble, D. 2014. Graphitic Carbon: A Ubiquitous, Diverse, and Useful Geomaterial. *Elements*, **10**, 415–420.

Bjørlykke, K. 2014. Relationships between depositional environments, burial history and rock properties. Some principal aspects of diagenetic process in sedimentary basins. *Sedimentary Geology*, **301**, 1–14.

Boggs, S. 2009. Petrology of Sedimentary Rocks, 2nd Edition, 612 pp. University of Oregon; Cambridge.

Bridge, J.S. 2003. Rivers and Floodplains: Forms, Processes, and Sedimentary Record, 512 pp. Blackwell; Oxford.

Buseck, P.R. and Beyssac. O. 2014. From Organic Matter to Graphite: Graphitization. *Elements*, **10**, 421–426.

Caracciolo, L. 2020. Sediment Generation and Sediment Routing Systems from a Quantitative Provenance Analysis Perspective. Review, Application and Future Development. *Earth-Science Reviews*, **209**, 103226.

Catuneanu, O. 2019. Model-independent sequence stratigraphy. *Earth-Science Reviews*, **188**, 312–388.

Chamley, H. 1989. Clay Sedimentology, 623 pp. Springer-Verlag; Berlin.

Choquette, P.W. and Pray, L.C. 1970. Geologic nomenclature and classification of porosity in sedimentary carbonates. *American Association of Petroleum Geologists Bulletin*, **54**, 207–250.

Collinson, J.D., Mountney, N.P. and Thompson, D.B. 2006. Sedimentary Structures, 3rd Edition, 292 pp. Terra Publishing; Harpenden.

Cornell, R. and Schwertmann, U. 2003. The Iron Oxides. Structures, Properties, Reactions, Occurrences and Uses. 2nd, completely revised and extended Edition, 664 pp. Wiley-VCH, Weinheim.

Dhannoun, H.Y., AL-Dabbagh, S.M. and Hasso, A.A. 1988. The Geochemistry of the Gercus Red Bed Formation of Northeast Iraq. *Chemical Geology*, **69**, 87–93.

Dickinson, W.R. and Gehrels, G.E. 2009. U-Pb Ages of Detrital Zircons in Jurassic Eolian and Associated Sandstones of the Colorado Plateau, Evidence for Transcontinental

Dispersal and Intraregional Recycling of Sediment. *GSA Bulletin*, **121**, 408–433.

Dickinson, W.R., Beard, L.S., Brakenridge, G.R., Erjavec, J.L., Ferguson, R.C., Inman, K.F., Knepp, R.A., Lindberg, F.A. and Ryberg, P.T. 1983. Provenance of North American Phanerozoic sandstones in relation to tectonic setting. *Geological Society of America Bulletin*, **94**, 222–235.

Dickinson, W.R. and Gehrels, G.E. 2009. Use of U-Pb ages of detrital zircons to infer maximum depositional ages of strata. A test against a Colorado Plateau Mesozoic database. *Earth and Planetary Science Letters*, **288**, 115–125.

Dill, H.G. 2020. A geological and mineralogical review of clay mineral deposits and phyllosilicate ore guides in Central Europe – A function of geodynamics and climate change. *Ore Geology Reviews*, **119**, 103304.

Folk, R.L. 1974. Petrology of Sedimentary Rocks, 194 pp. Hernphill Publishing Co.; Austin.

Galán, E. and Pozo, M. 2011. Palygorskite and sepiolite deposits in continental environments. Description, genetic patterns and sedimentary settings. *Developments in Clay Science*, **3**, 125–173.

Galán, E. and Singer, A. 2011. Developments in Palygorskite-Sepiolite Research. A New Outlook on These Nanomaterials. *Developments in Clay Science*, **3**, 1–520.

Garzanti, E. 2016. From static to dynamic provenance analysis – Sedimentary petrology upgraded. *Sedimentary Geology*, **336**, 3–13.

Garzanti, E., Andò, S. and Vezzoli, G. 2007. Settling equivalence of detrital minerals and grain-size dependence of sediment composition. *Earth and Planetary Science Letters*, **273**, 138–151.

Hama Salih, T.M., Surdashy, A.M., Hama Salih, H.M. and Baziany, M.M. 2022. Facies Implication of Gercus Formation with the Bathymetry and Tectonic Activity of Van-Pyrenean Phases in Haibat-Sultan Mountain, Iraqi Kurdistan Region. *Qalaai Zanistscientific Journal*, **7**, 972–997.

Henares, S., Donselaar, M.E. and Caracciolo, L. 2020. Depositional controls on sediment properties in dryland rivers: Influence on near-surface diagenesis. *Earth-Science Reviews*, **208**, 103297

Hillier, S. 1995. Erosion, sedimentation and sedimentary origin of clays. In: Farmer, V.C. and Douglas, T.J. (Eds), Origin and Mineralogy of Clays: Clays and the Environment, 162–219. Springer; Berlin.

Hussain, S.H. and Aghwan, T.A. 2014. Sedimentology and evolution of a foreland desert basin, Middle Eocene Gercus Formation (North and Northeastern Iraq). *Arabian Journal of Geosciences*, **8**, 2799–2830.

Jahren, J.S. and Aagaard, P. 1989. Compositional variations in diagenetic chlorites and illites, and relationships with formation-water chemistry. *Clay Minerals*, **24**, 157–170.

Jassim, S.Z. and Goff, J.C. 2006. Geology of Iraq, 341 pp. Dolin, Prague and Moravian Museum; Brno.

Jones, B.F. and Galán, E. 2008. Palygorskite and sepiolite. In Hydrous Phyllosilicates (Exclusive of Micas). *Reviews in Mineralogy and Geochemistry*, **19**, 631–674.

Kadhum, M.A. and Habib, H.R. 2015. Mineralogy of palygorskite-rich claystone in Gercus formation, dohuk governorate, northern Iraq. *Iraqi Bulletin of Geology and Mining*, **11**, 75–91.

Karim, H.K., Baziany, M.M. and Khanaqa, P. 2018. New Ideas and Critical review of Middle Eocene Gercus Formation, Kurdistan Region, NE-Iraq. *Journal of Zankoy Sulaimani, (JZS)*, **20**, 81–94.

Karim, K.H., Khanaqa, P.A. and Babashekh, S.M. 2020. Revisiting the Gercus Basalt within the Eocene Gercus Formation: Implications for sedimentary origin of a basaltic body, Kurdistan Region, Northern Iraq, 4–5. Ore and Energy Resource Geology; Amsterdam.

Kehl, M., Vlaminck, S., Köhler, T., Laag, C., Rolf, C., Tsukamoto, S., Frechen, M., Sumita, M., Schmincke, H. and Khormali. F. 2021. Pleistocene dynamics of dust accumulation and soil formation in the southern Caspian Lowlands – New insights from the loess-paleosol sequence at Neka-Abelou, northern Iran, 253 pp. Quaternary Science Reviews, Oxford.

Kettanah Y.A., Armstrong-Altrin J.S. and Mohammad F.A. 2020. Petrography and geochemistry of siliciclastic rocks of the Middle Eocene Gercus Formation, northern Iraq: Implications for provenance and tectonic setting. *Geological Journal*, **56** (5), 1–22.

Kettanah, Y.A. and Bamarni, A.M. 2018. Petrogenesis, geochemistry, and tectonic setting of a basaltic body within the Gercus Formation of northern Iraq. First record for Eocene anorogenic volcanic activity in the region. *Turkish Journal of Earth Sciences*, **27**, 460–491.

Khadkikar, A.S., Merh, S.S., Malik, J.N. and Chamyal, L.S. 1998. Calcretes in semi-arid alluvial systems: formative pathways and sinks, *Sedimentary Geology*, **116**, 251–260.

Klappa, C.F. 1980. Rhizoliths in terrestrial carbonates: Classification, recognition, genesis and significance. *Sedimentology*, **27**, 613–629.

Knighton, A.D. and Nanson, G.C. 1994a. Flow transmission along an arid-zone anastomosing river, Cooper Creek, Australia. *Hydrological Processes*, **8**, 137–154.

Knighton, A.D. and Nanson, G.C. 1994b. Waterholes and their significance in the anastomosing channel system of Cooper Creek, Australia. *Geomorphology*, **9**, 311–324.

Kraus, M.J. and Aslan, A. 1993. Eocene hydromorphic paleosols: Significance for interpreting ancient floodplain processes. *Journal of Sedimentary Research*, **63**, 453–463.

Kraus, M.J. 1999. Paleosols in clastic sedimentary rocks: Their geologic applications. *Earth-Science Reviews*, **47**, 41–70.

Kraus, M.J. and Hasiotis, S.T. 2006. Significance of different modes of rhizolith preservation to interpreting paleoenvironmental and paleohydrologic settings. Examples from

Paleogene paleosols, Bighorn Basin, Wyoming, USA. *Journal of Sedimentary Research*, **76**, 633–646.

Liu, Q., Roberts, A.P., Larrasoaña, J.C., Banerjee, S.K., Guyodo, Y., Tauxe, L. and Oldfield, F. 2019. Environmental magnetism: Principles and applications. *Reviews of Geophysics*, **57**, 123–194.

Luque, F.J., Ortega, L., Barrenechea, J.F., Millward, D. and Beyssac, O. 2014. Deposition of organic matter in the Proterozoic and its transformation into graphite. *International Journal of Earth Sciences*, **103**, 1713–1732.

Luque, F.J., Pasteris, J.D., Wopenka, B., Rodas, M. and Barrenechea, J.F. 1998. Natural fluid-deposited graphite: mineralogical characteristics and mechanisms of formation. *American Journal of Science*, **298**, 471–498.

Machel, H.G. 2004. Concepts and Models of Dolomitization. A Critical Reappraisal. *Geological Society of London Special Publication*, **235**, 7–63.

Mack, G.H., Cole, D.R. and Trevin, O.L. 2000. The distribution and discrimination of shallow, authigenic carbonate in the Pliocene Pleistocene Palomas Basin, southern Rio Grande rift. *Geological Society of America Bulletin*, **112**, 643–656.

Makaske, B. 2001. Anastomosing rivers: a review of their classification, origin and sedimentary products. *Earth-Science Reviews*, **53**, 149–196.

Makaske, B., Lavooi, E., De Haas, T., Kleinhans, M.G. and Smith, D.G. 2017. Upstream Control of River Anastomosis by Sediment Overloading, Upper Columbia River, British Columbia, Canada. *Sedimentology*, **64**, 1488–1510.

Malak, Z.A., Al-Banna, N. Y. and Al-Mutwali, M. M. 2019. The provenance of Eocene sandstones (Gercus Formation), Northern Iraq. *Iraqi National Journal of Earth Sciences*, **19**, 57–68.

Maroulis, J.C., Nanson, G.C., Price, D.M. and Pietsch, T. 2007. Aeolian–fluvial interaction and climate change: source-bordering dune development over the past ~100 ka on Cooper Creek, central Australia. *Quaternary Science Reviews*, **26**, 386–404.

Marsaglia, K.M. and Ingersoll, R.V. 2018. Compositional trends in arc-related, deep-marine sand and sandstone. A reassessment of magmatic-arc provenance. *Geological Society of America Bulletin*, **130**, 1722–1750.

McCarthy, P.J. and Plint, A.G. 1998. Recognition of interfluve sequence boundaries. Integrating paleopedology and sequence stratigraphy. *Geology*, **26**, 387–390.

Métais, G., Barrier, E., Muller, C. and Sen, S. 2014. The Red Clastics of the Early–Middle Eocene Gercus Formation in South East Turkey and Northern Iraq. Lithofacies and Depositional Environments. Final Symposium, Abstracts Volume. December 8–9, 2014, 90–91. University Pierre and Marie Curie; Paris.

Meunier, A. 2005. Clays, 472 pp. Springer-Verlag; Berlin.

Miall, A.D. 1996. The Geology of Fluvial Deposits. Sedimentary Facies, Basin Analysis, and Petroleum Geology, 582 pp. Springer-Verlag; Berlin.

Miall, A.D. 1985. Architectural-element analysis: A new method of facies analysis applied to fluvial deposits. *Earth-Science Reviews*, **22**, 261–308.

Miall, A.D. 2006. The Geology of Fluvial Deposits: Sedimentary Facies, Basin Analysis, and Petroleum Geology (Reprint Edition), 582 pp. Springer-Verlag; Berlin.

Miall, A.D. 2014. Fluvial Depositional Systems, 316 pp. Springer; Cham.

Miall, A.D. 2016. Stratigraphy: A Modern Synthesis, 454 pp. Springer; Cham.

Milliken, K.L. and Mack, L.E. 2003. Integration of SEM, XRD, and chemical data in the characterization of detrital and diagenetic minerals in shales. *Journal of Sedimentary Research*, **73**, 871–883.

Millot, G. 1970. Geology of Clays. Weathering, Sedimentology, Geochemistry, 429 pp. Springer-Verlag; New York.

Moore, D.M. and Reynolds, R.C. 1997. X-ray Diffraction and the Identification and Analysis of Clay Minerals. 2nd Edition, 378 pp. Oxford University Press; Oxford.

Morad, S. 1998. Carbonate cementation in sandstones. Distribution patterns and geochemical evolution. In: Morad, S. (Ed.), Carbonate Cementation in Sandstones, 1–26. Blackwell Science; Oxford.

Morad, S., Al-Ramadan, K., Ketzer, J.M. and De Ros, L.F. 2012. The impact of diagenesis on the heterogeneity of sandstone reservoirs. A review of the role of depositional facies and sequence stratigraphy. *AAPG Bulletin*, **96**, 341–377.

Nanson, G.C. 2013. Anabranching and anastomosing rivers. *Earth System and Environmental Sciences*, **9**, 330–345.

Nanson, G.C. Rust, B.R. and Taylor, G. 1986. Coexistent mud braids and anastomosing channels in an arid-zone river: Cooper Creek, central Australia. *Geology*, **14**, 175–178.

Nasif, A.K. and Khwedim, K.H. 2022. Heavy Mineral Distribution of Gercus Formation in Shaqlawa and Dokan Area in Northern Iraq. *Academic Science Journal*, **1**, 77–93.

Nichols, G. 2023. Sedimentology and Stratigraphy, 3rd Edition, 544 pp. Wiley-Blackwell; Hoboken, New Jersey.

Numan, N.M.S. 1997. A plate tectonic scenario for the Phanerozoic succession in Iraq. *Journal of the Geological Society, Iraq*, **30**, 85–110.

Nusaif, A.K. and Khwedim, K.H. 2023. Petrography of Sandston Units in Gercus Formation, Shaqlawa and Dokan areas Northern Iraq. *Iraqi Journal of Science*, **64**, 1799–1809.

Posamentier, H.W. and Walker R.G. (Eds) 2006. Facies Models Revisited. SEPM Special Publication No. 84. SEPM Society for Sedimentary Geology; Tulsa.

Potter, D.K., Corbett, P.W., Barclay, S. and Haszeldine, R.S. 2004. Quantification of Illite Content in Sedimentary Rocks Using Magnetic Susceptibility – A Rapid Complement or Alternative to X-Ray Diffraction. *Journal of Sedimentary Research*, **74**, 730–735.

Reading, H.G. 1996. Sedimentary environments: Processes, facies and stratigraphy, 689 pp. Blackwell Science; Oxford.

Reineck, H.E. and Singh, I.B. 1980. Depositional Sedimentary Environments: With Reference to Terrigenous Clastics, 2nd Edition, 551 pp. Springer Study Edition, Springer-Verlag; Berlin.

Retallack, G.J. 2001. Soils of the Past. An Introduction to Paleopedology, 404 pp. Blackwell Science; Oxford.

Royer, D.L. 1999. Depth to pedogenic carbonate horizon as a paleoprecipitation indicator? *Geology*, **27**, 1123–1126.

Salvador, A. 2013. International Stratigraphic Guide: A Guide to Stratigraphic Classification, Terminology, and Procedure. 2nd Edition, 214 pp. Geological Society of America; Boulder.

Schmid, S., Worden, R.H. and Fisher, Q.J. 2004. Diagenesis and reservoir quality of chlorite-bearing sandstones. *AAPG Bulletin*, **88**, 997–1017.

Schumm, S.A. 1968. Speculations Concerning Paleohydrologic Controls of Terrestrial Sedimentation. *GSA Bulletin*, **79**, 1573–1588.

Scotese, C.R. 2014. Atlas of Paleogene Paleogeographic Maps (Mollweide Projection). Maps 8–15, Volume 1, the Cenozoic, PALEOMAP Atlas for ArcGIS. PALEOMAP Project, Evanston, IL. Technical Report; Evanston, IL.

Sharland, P.R., Archer, R., Casey, D.M., Dvis, R.B., Hall, S., Heward, A., Horbury, A. and Simmons, M.D. 2001. Arabian Plate Sequence Stratigraphy. GeoArabia, Special Publication, 2, 389 pp. Gulf Pertolink; Bahrain.

Sheldon, N.D. and Tabor, N.J. 2009. Quantitative paleoenvironmental and paleoclimatic reconstruction using paleosols. *Earth-Science Reviews*, **95**, 1–52.

Singer, A. 1989. Palygorskite and sepiolite group minerals. In: Dixon, J.B. and Weed, S.B. (Eds), Minerals in Soil Environments, 2nd Edition, 829–872. Soil Science Society of America Book Series 1, Madison, Wisconsin.

Singer, A. 2002. Palygorskite and sepiolite group minerals. In: Dixon, J.B. and Schulze, D.G. (Eds) Soil Mineralogy with Environmental Applications, 291–322. Soil Science Society of America; Madison.

Singer, A. 2002. Palygorskite. In: Jambor, J.L., Vaughan, D.J. and Brownlow, A.H. (Eds), Reviews in Mineralogy and Geochemistry. *Mineralogical Society of America*, **19**, 555–583.

Sissakian, V.K. and Fouad, S.F. 2015. Geological Map of Iraq, scale 1: 1000 000, 4 th Editiondit. 2012 GEOSURV, Baghdad, Iraq. *Iraqi Bulletin of Geology and Mining*, **11**, 9–16.

Slingerland, R. and Smith, N.D. 2004. River Avulsions and Their Deposits. *Annual Review of Earth and Planetary Sciences*, **32**, 257–285.

Smith, D.G. 1983. Anastomosed fluvial deposits: modern examples from West Canada. *Sedimentology*, **6**, 155–168.

Smith, N.D., Cross, T.A., Dufficy, J.P. and Clough, S.R. 1989. Anatomy of an avulsion. *Sedimentology*, **36**, 1–23.

Smith, D.G. and Smith, N.D. 1980. Sedimentation in anastomosed river systems: examples from alluvial valleys near Banff, Alberta. *Journal of Sedimentary Petrology*, **50**, 157–164.

Soua, M. 2025. Middle Permian Depositional Environments Inferred from Illite Crystallinity and Illite Chemistry Indices of X-Ray Diffraction Patterns. Saudi Arabia, Conference, Middle East Oil, Gas and Geosciences Show (MEOS GEO), SPE-227177-MS. Society of Petroleum Engineers (SPE); Manama.

Southard, J.B. 1991. Experimental Determination of Bed-Form Stability. *Annual Review of Earth and Planetary Sciences*, **19**, 423–455.

Środon, J., Szulc, J., Anczkiewicz, A., Jewuła, K., Banaś, M. and Marynowski, L. 2014. Weathering, sedimentary and diagenetic controls of mineral and geochemical characteristics of the vertebrate-bearing Silesian Keuper. *Clay Minerals*, **49**, 569–594.

Środoń, J., Zeelmaekers, E. and Derkowski, A. 2009. The charge of component layers of illite-smectite in bentonites and the nature of end-member illite. *Clays and Clay Minerals*, **57**, 649–671.

Tabor, N.J. and Myers, T.S. 2015. Paleosols as indicators of paleoenvironment and paleoclimate. *Annual Review of Earth and Planetary Sciences*, **43**, 333–361.

Thiry, M. 2000. Palaeoclimatic interpretation of clay minerals in marine deposits: An outlook from the continental origin. *Earth-Science Reviews*, **49**, 201–221.

Thiry, M. and Jacquin, T. 1993. Clay mineral distribution related to rift activity, sea-level changes and paleoceanography in the Cretaceous of the Atlantic Ocean. *Clay Minerals*, **28**, 61–84.

Tooth, S. 2013. Dryland fluvial environments: assessing distinctiveness and diversity from a global perspective. *Geological Society, London, Special Publications*, **376**, 61–88.

Tucker, M.E. 2023. Sedimentary Petrology: An Introduction to the Origin of Sedimentary Rocks (4th Edition), 448 pp. Wiley-Blackwell; Hoboken.

Tucker, M.E. and Wright, V.P. 2009. Carbonate Sedimentology (2nd Edition), 482 pp. Wiley-Blackwell; Oxford.

Turner, P. 1980. Continental Red Beds. Developments in Sedimentology 29, 562 pp. Elsevier; Amsterdam.

Velde, B. 1995. Composition and Mineralogy of Clay Minerals. In: Velde, B. (Ed.), Origin and Mineralogy of Clays: Clays and the Environment, 8–42. Springer; Berlin.

Walker, R.G. and James, N.P. 1992. Facies Models Response to Sea Level Change, 407 pp. Geological Association of Canada; St. John's, Newfoundland.

Walker, T.R. 1967. Formation of red beds in modern and ancient deserts. *Geological Society of America Bulletin*, **78**, 353–368.

Warren, J. 2000. Dolomite: Occurrence, Evolution and Economically Important Associations. *Earth-Science Reviews*, **52**, 1–81.

Watts, N.L. 1980. Quaternary pedogenic calcretes from the Kalahari (southern Africa): Mineralogy, genesis and diagenesis. *Sedimentology*, **27**, 661–686.

Weaver, C.E. and Beck, K.C. 1977. Miocene of the S.E. United States. A model for chemical sedimentation in a peri-marine environment. *Sedimentary Geology*, **17**, 1–234.

Weltje, G.J. and von Eynatten, H. 2004. Quantitative provenance analysis of sediments: review and outlook. *Sedimentary Geology*, **171**, 1–11.

Wilson, M.J. 2013. Rock-Forming Minerals: Sheet Silicates, Clay Minerals (Vol. 3C), 724 pp. The Geological Society; London.

Worden, R.H. and Morad, S. 2003. Clay minerals in sandstones: controls on formation, distribution, and evolution. *International Association of Sedimentologists Special Publication*, **34**, 3–41.

Wright, V.P. 2007. Calcretes. In: Nash, D.J., and McLaren, S.J. (Eds), Geochemical Sediments and Landscapes, 10–45. Blackwell Publishing Ltd; Oxford.

Wright, V.P. and Tucker, M.E. 1991. Calcretes. International Association of Sedimentologists Reprint Series Volume 2, 352 pp. Blackwell Scientific Publications; Oxford.

Yeganeh, B.Z., Feiznia, S. and Van Loon, A.J. 2012. Sedimentary environment and palaeogeography of the Palaeocene–Middle Eocene Kashkan Formation, Zagros fold-thrust belt, SW Iran. *Geologos*, **18**, 13–36.

Ylagan, R.F., Altaner, S.P. and Pozzuoli, A. 2000. Reaction mechanisms of smectite illitization associated with hydrothermal alteration from Ponza Island, Italy. *Clays and Clay Minerals*, **48**, 610–631.

Manuscript submitted: 18th December 2025
Revised version accepted: 10th June 2026